

Egyptian Journal of Geology

https://egjg.journals.ekb.eg



Assessing Radiological Hazards and Spatial Distribution of Natural Radioactivity in the Suez Region (Egypt) through Ground–Airborne Gamma-Ray and GIS Integration



B. Abdo¹, A. M. Saad¹, M. A. H. Sakr¹ and A. E. Omar²

RADIOLOGICALLY focused geo-environmental study was conducted in Egypt's Suez region Aand its surrounding areas to evaluate the presence and distribution of both naturally occurring and anthropogenic radionuclides within soil layers at varying depths. A total of 87 soil samples were collected, 29 each from depths 0.5, and 10 m., the concentrations of natural radionuclides (238U, 232Th, and ⁴⁰K) were measured using High-Purity Germanium (HPGe) γ-ray spectrometry. Radiation hazard indicators such as radium equivalent activity, gamma index, internal and external hazard indices, annual effective dose (both indoor and outdoor), and absorbed dose rate were systematically evaluated. For surface-level soil samples (0 meters), radium equivalent activity varied between 50 and 100 Bq/kg, with an average of 75 Bq/kg. The gamma index ranged from 0.29 to 0.80 (mean 0.55); while the internal hazard index spanned 0.27 to 0.97 (mean 0.62). The estimated annual indoor effective dose ranged from 0.18 to 0.52 mSv/year (mean 0.35) and absorbed dose rates were between 37 and 106 nGy/hour (mean 72). A gradual increase in these parameters was noted with depth, reaching peak values in samples derived from airborne gamma-ray data where radium equivalent activity reached up to 609 Bq/kg (mean 385), and absorbed dose rate peaked at 280 nGy/hour (mean 180). This multidisciplinary investigation, incorporating both ground-based sampling and airborne survey techniques, delivers an extensive dataset detailing the spatial distribution of radionuclides and related radiological risks across the Suez region. The findings contribute valuable insights for environmental surveillance, hazard evaluation, and the development of radiation safety measures along the Gulf of Suez.

Keywords: Radiological Hazards, Natural Radioactivity, Ground–Airborne Gamma-Ray Survey, GIS, Spatial Distribution, Suez Region, Egypt.

1. Introduction

Radioactivity is naturally present in a wide range of environments, including rocks, soils, beach sands, sediments, and riverbeds, as well as in rivers, oceans. construction materials. residential buildings, and even subsurface locations (Ravisankar et al., 2015& Ambrosino et al., 2020a). Natural sources contribute nearly 80% of the total annual effective radiation dose received by humans (UNSCEAR, 2010). The primary contributors to environmental radiation primordial radionuclides, which are long-lived isotopes that have persisted since the Earth's formation (Abd El Rahman et al., 2022). The type and composition of rocks and soils play a key role in controlling the

spatial distribution of these radionuclides (Gaafar et al., 2021& Forkapic et al., 2017). Moreover, radionuclides can migrate from geological materials to humans through different pathways (such as emanation and exhalation), thereby increasing the risk of harmful radiation exposure to the population (Jakhu et al., 2018).

Background radiation refers to the omnipresent ionizing radiation to which humans are continuously exposed, originating from both natural and artificial sources. Daily, radionuclides enter the human body through the air we breathe, the food we consume, and the water we drink. Generally speaking, radiation is present everywhere (Uosif &

*Corresponding author e-mail: geo.belalabdou11315@yahoo.com

Received: 16/09/2025; Accepted: 05/10/2025 DOI: 10.21608/EGJG.2025.424349.1128

©2025 National Information and Documentation Center (NIDOC)

¹Geology department- Faculty of science- Al-Azhar University, Egypt

²Nuclear Materials Authority, Cairo, Egypt

Abdel-Salam, 2011). Studying radioactivity in the environment is crucial for assessing potential radiological risks to humans and other living organisms, as well as for providing essential information to monitor contamination and guide radiation protection policies. Measuring radioactivity in soils is not limited to determining radionuclide levels but also includes calculating radiation hazard indices such as radium equivalent activity, absorbed dose rate, and internal and external hazard indices. This data allows the creation of a comprehensive database of the radiological environment, which is a crucial step toward safeguarding public health and supporting sustainable development in areas exposed to natural or anthropogenic radiation (Eke et al., 2024). Background of natural radiation levels in each environment is required to understand better human exposure to natural radiation from a radiation safety viewpoint (Briestensky et al., 2022). The 238U, 226Ra, 232Th, and 40 K are the main radionuclides forming the natural radiation, with worldwide average activity concentrations in soils of 33 Bq·kg-1, 32 Bq·kg-1, 45 Bq·kg-1, and 412 Bq·kg-1 respectively (Gaafar et al., 2021). Global average exposure rate from terrestrial gamma rays have been found to be around 59 nGy·h-1 (UNSCEAR Sources and Effects Of, 2010), and the terrestrial background radiation is directly dependent on the geological formation of the places (D'Avino et al., 2022). Radioactive contamination is the deposition or presence of radioactive materials on surfaces or within solids, liquids or gases (including the human body), where their presence is unintentional or undesirable (IAEA Annual Report, 2007).. This pollution poses a danger because the radioactive decay of pollutants produces harmful ionizing radiation, including alpha, beta, and gamma rays. The degree of danger is determined by the concentration of pollutants, the energy of the emitted radiation, the type of radiation, and the proximity of the pollution to the body's organs. Long-term exposure to U, Ra, and their decay products cause significant ailments including chronic lung disease, oral necrosis, leukopenia, and anaemia (Taylor and Owens, 2009; Forkapic et al., 2017 and IAEA Annual Report 2007). Exposure to

radionuclides may lead to the development of cancers in vital organs such as the liver, kidneys, bones, lungs, and pancreas. These radionuclides are introduced and dispersed into the environment primarily through anthropogenic activities, including uranium mining (Ambrosino et al., 2019). Numerous studies have been carried out to assess natural radioactivity for various applications, such as ensuring safe urban expansion, evaluating mining operations, and examining rocks utilized in construction and decorative purposes (Sakr et al., 2021; Saad et al., 2020; La Verde et al., 2020 and Omar et al., 2021). In this context, the current study aimed to evaluate the natural radiological risk in Egypt's Suez region.

Radioactivity represents a natural hazard and a potentially harmful phenomenon that may lead to loss of life, injuries, property damage, infrastructure deterioration, and disruptions in social and economic systems. Each rock type exhibits a characteristic level of radioactivity, generally referred to as its normal or background radiation. A significant rise in radioactivity, exceeding the background value of a given rock type by fivefold or more, is regarded as an anomaly.

In the present work the GIS was employed to store, manage, and analyze the collected radiometric datasets, and to generate thematic maps that clearly illustrate the spatial variability of radioactivity across the study area. These maps facilitated the identification of anomalous zones, interpretation of their spatial relationship with lithological and structural features and provided a geospatial framework for evaluating the potential radiological hazards Geographic Information Systems (GIS) are designed to store, manage, and retrieve various types of data linked to specific geographic locations (Dangermond, 1984; Gupta, 1991) Geospatial methodologies have been widely applied in numerous fields, including mineral exploration, flash flood risk assessment, radioactive hazard evaluation. urban development, and environmental studies (Omar, 2016, 2021; Omar et al., 2016a, b; Arnous & Omar, 2018; and Saad et al., 2020). In this context, integrating GIS techniques within the present study improved the

visualization and interpretation of radioactive distribution patterns, representing a key step toward environmental risk evaluation and sustainable landuse planning in the Suez region.

The present study uses airborne gamma-ray spectrometric data along with 87 collected soil samples to assess the radiation hazards in the Suez region, Egypt. The concentrations of natural radionuclides (238U, 232Th, 40K) were measured, and radiation hazard parameters, including radium equivalent activity, gamma index, internal and external hazard indices, absorbed dose rate, and annual effective dose (indoor and outdoor), were calculated and analyzed to delineate potential hazards caused by the distribution of natural radionuclides.

The objective of this research is to evaluate the radiological background and geo-environmental characteristics of the Suez region through the measurement and spatial distribution of natural radioactivity levels in different rocks and soils, as well as the identification of radiological anomalies associated with geological structures. The study relies on the application of remote sensing and GIS techniques to generate spatial distribution maps and geo-environmental models that enable the analysis of the relationship between radiological distribution and geological factors. This, in turn, contributes to assessing potential radiological hazards and supporting sustainable development strategies in the region.

2. Study area characteristics

The study area is located in the Suez region, in the northern part of the Gulf of Suez, Egypt, where the Suez Canal connects with the gulf (Fig. 1). It extends geographically between latitudes 29°58′ and 30°9′ N and longitudes 32°25′ and 32°45′ E. It is bounded to the west by the rugged highlands of Gabal Ataqa, and to the east it extends across the Suez Canal to include part of the Sinai Peninsula. This area was chosen due to its strategic importance as a vital gateway linking Sinai with mainland Egypt. At present, the region is witnessing rapid urban expansion and large-scale infrastructure development, which makes it necessary to assess its geological, geotechnical, and geo-environmental

characteristics, as well as potential radiological hazards, to ensure safe and sustainable development planning. The proposed zone for urban development occupies gently sloping and slightly dissected terrain, which rises gradually toward the west and northwest, culminating at the base of the steep escarpments of Gabal Ataqa. The mean elevation above sea level is approximately 12 m

The upland sector corresponds to the uplifted limestone plateau of Gabal Ataqa, reaching 871 m in height, which significantly shapes the region's geomorphological characteristics. By contrast, the lowland areas extend eastward across the isthmus. The drainage system is primarily fed by runoff from the northern flanks of Gabal Ataqa, forming wadis and ephemeral streams that generally flow eastward. The total area encompasses about 9,002 km². The principal geomorphological units of the Suez region include beaches and raised marine deposits, offshore bars and fringes, coastal accumulations, fluvial deposits, Miocene bedrock exposures, and anthropogenic ally developed zones (Bush et al., 1980; Mahfouz, 1999; and Arnous, 2004).

. Climatic conditions in the study area are typical of North Africa's arid zones. The Suez Canal region experiences a subtropical climate, marked by hot summers and mild winters. On an annual scale, the climate is affected by both desert influences and Mediterranean moderation Based on weather reports collecting during the periods of 1958 to 2015, The average annual temperature in the study area ranging from 10.5 to 36.1 degree Celsius (°C) August is recorded as the hottest month while the coldest one is January. Dry drainage lines dissect the surface of the study area, which are directed into the major basins to the Gulf of Suez. These wadis are intermittently activated during periods of rainfall. In general, the area under investigation is characterized by arid climatic conditions, dominated by a long hot rainless summer and a mild winter. The most precipitation occurs in the form of heavy showers of a short duration especially in the period from December to April/year (Omran 2006).

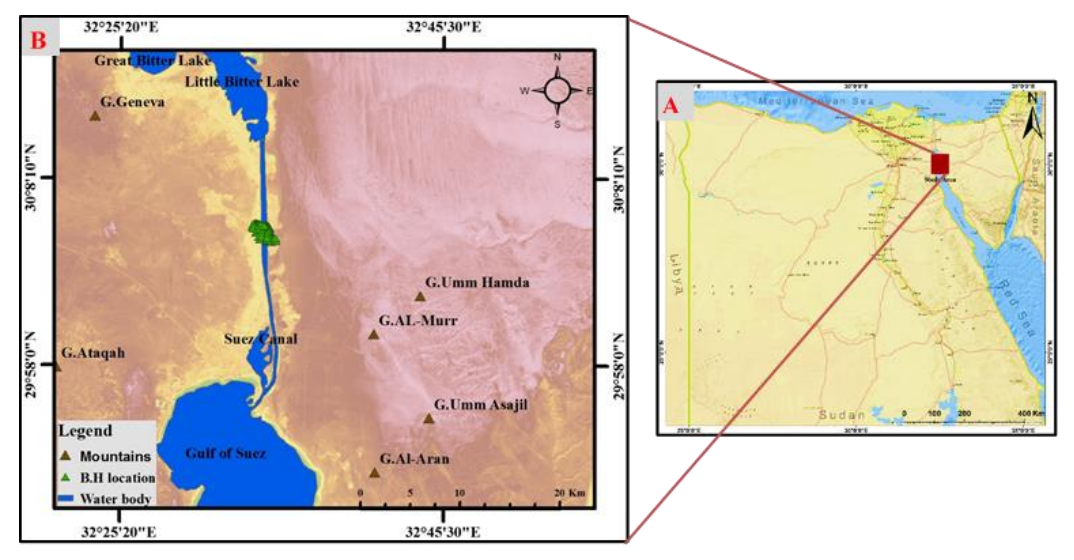


Fig. 1. (A) Study area location in relation to Egypt (B) Suez area location in relation to Egypt.

The average annual rainfall 17 mm but it is extremely variable and average temperature of 22.5°C. Wind predominately blows from N, NE, or NW directions and the mean annual wind speed is 4.6 knots. The study area is highly evaporated and has an annual daily mean of 9.4 mm, the clouds and fogs are common at nighttime and early morning and give rise to regular fall (Egyptian Metrological Authority 1996). Due to human and industrial activities, the Suez Canal Zone suffered from relatively higher humidity levels. The average annual relative humidity in Suez is 53.3 %. The wind patterns in the Suez Canal Zone play a crucial role in navigation and transportation operations, particularly during periods of reduced visibility or sandstorms. Understanding the wind speed and air density variations is essential for assessing the potential risks and challenges faced by ships transiting through the canal. Over the investigated zone, the wind speed ranges from 5 to 11.9 m/s, while the density of air graduated from 1.07 to 1.23 kg/m3 (Effat, 2017).

3. Geological setting of the study area

The Suez region is characterized by a thick sedimentary succession that spans from the Eocene to the Quaternary (Fig. 2), the Surface of the study area is generally flat, dissected by wadis filled with alluvial deposits, and shows ripple marks reflecting fluvio-marine activity. Based on ASTER satellite data processing using Principal Component Analysis (PCA), the area and its surroundings are shown to be dominated by sedimentary rocks of fluvio-marine origin distributed widely across the region. The sequence begins with Eocene rocks, which are widely exposed in the Northeastern Desert and have been

studied in detail by many authors (e.g. AbdElshafy et al., 1989; Strougo & Abdallah, 1990; Abu El-Enain et al., 1995; Bignot & Strougo, 2002). The Upper Eocene is represented by the Maadi Formation, consisting mainly of limestone, soft marls, and gritty sandstone beds (Arnous et al., 2023).

Overlying these deposits are Oligocene sediments, consisting of diverse clastic deposits such as sands, gravels, and silts, which are related to the activity of ancient drainage systems that once influenced the region (El Shazly et al., 1975). Southward, Miocene rocks are well represented, including the Hagul Formation, which is made up of sandstone, clay, and limestone, and the Hommath Formation, which is dominated by limestone interbedded with clay and sandstone (Abdalla and Abdel Hady, 1966). At Gebel Ataqa, the Miocene sequence was subdivided into the Suez Formation at the base and the Ramiya Formation at the top (El Akkad and Abdallah, 1971). The Quaternary deposits form the most extensive cover, reaching more than 200 meters in thickness. These deposits include braided river sediments to the north and fan-shaped accumulations at the mouths of valleys to the east. Subsurface investigations revealed a lower unit of coarse, clay-free sands overlain by fine sands interbedded with clay and silt (Abdallah et al., 1998). These deposits are widely distributed and resemble the cultivated muddy soils of the Nile Delta.

Structurally, the geology of Suez is closely linked to the evolution of the Suez Rift.

This rift extends for about 350 km in a NNW direction with an average width of 90 km, and today it represents an inactive continental rift separating the African plate from the Sinai microplate (Said, 1962; and Moustafa, 2002).

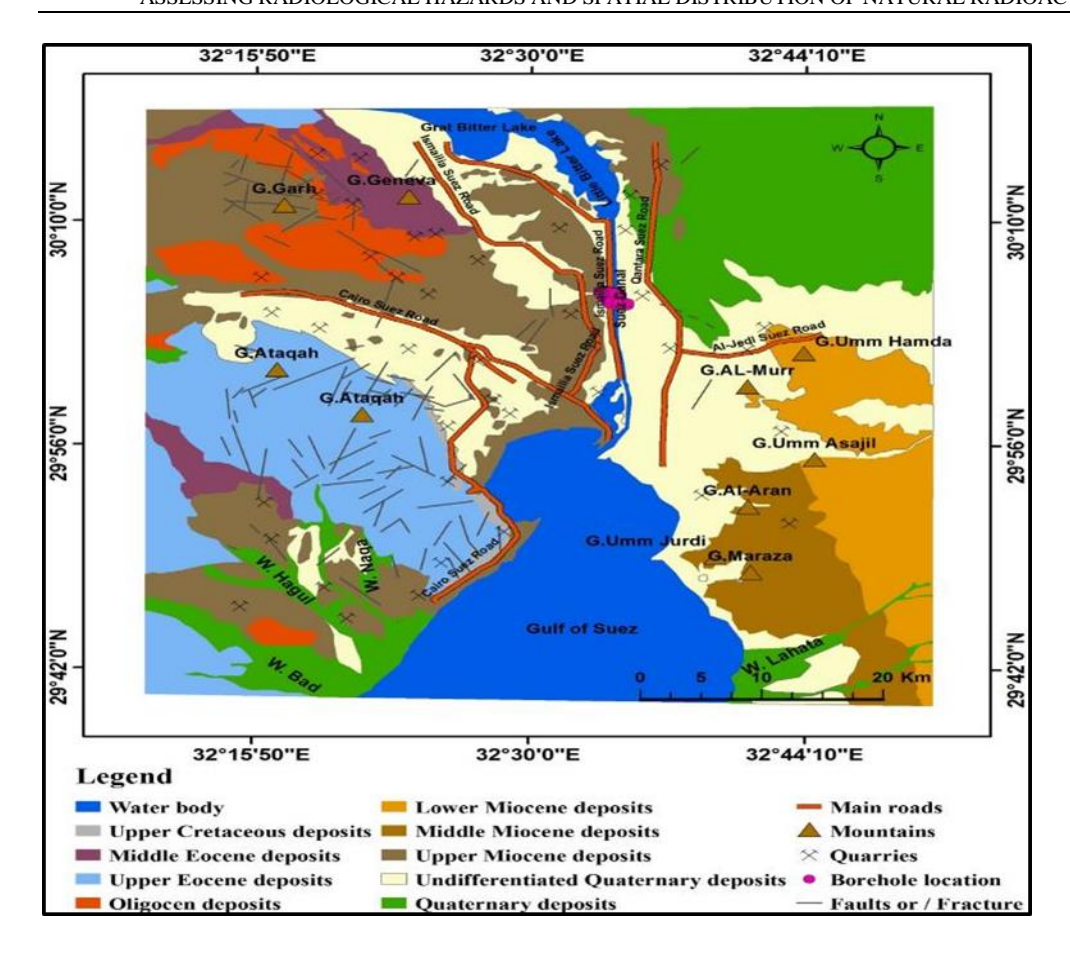


Fig. 2. Geological map of the study area (Modified after Conoco, 1987).

One of the most prominent features is the Hagul Fault, a NW-SE trending lineament along the western margin of the region, clearly exposed in Wadi Hagul (Gargani & Moretti, 2008). Regionally, tectonic activity in the Suez area is influenced by the Red Sea-Gulf of Suez rifting, left-lateral strike-slip motion along the Gulf of Aqaba-Levant transform, and the convergence between the African and Eurasian plates in the eastern Mediterranean (Ben-Avraham et al., 1987). From a neotectonic perspective, Suez region is considered one of the most seismically active areas in Egypt, with shallow to intermediate magnitude earthquakes concentrated along the Gulf of Suez-Cairo-Alexandria active seismic trend (Abou Elenean, 1997).

4. Materials and Methods

4. 1. Samples Collection and Preparation

In the present study, the assessment of natural radioactivity in the investigated area was carried out through two complementary approaches. The first involved the collection of soil samples at different depths (0, 5, and 10 meters) using rotary drilling (Fig. 3), where detailed gamma spectrometric analyses

performed to determine the activity concentrations of uranium, thorium, and potassium. These ground-based measurements provided accurate point data reflecting the vertical distribution of natural radionuclides. The second approach utilized airborne spectrometric maps, from gamma-ray radiometric data were extracted and used to construct detailed distribution maps for the study area. To support both approaches, Geographic Information System (GIS) techniques were applied to process, analyze, and visualize the spatial datasets. ArcGIS software (version 10.8) was employed to prepare the location map, compile the geological map from published sources (e.g., Conoco, 1987), and generate spatial distribution maps of uranium, thorium, and potassium. The integration of ground sampling, airborne datasets, and GIS-based mapping enabled a comprehensive evaluation of the radiological characteristics of the area, combining high-resolution local measurements with broader regional coverage.

4. 1.1. Ground Radiometric Analysis

This part includes the collection of soil samples from the study area at different depths (0, 5, and 10 meters)

by rotary drilling method, following the standard procedures recommended for soil sampling (IAEA, 1989) followed by the required radiometric analyses to determine the activity concentrations of uranium, thorium, and potassium.

A total of 87 soil samples, comprising 60 clay and 27 sand, were collected at depths of 0, 5, and 10 m. Boreholes were systematically drilled across the study area at predetermined intervals, from which the samples were retrieved for subsequent radiological analyses. The sampling strategy was designed to be random but guided by lithological variations, thereby ensuring a representative coverage of the entire study area. Soil samples were dried in an oven at 100° to determine the moisture content until a constant weight was obtained. The dried samples were pulverized and sieved to pass through a coarse mesh (1-2 mm size fraction). Soil samples were collected by the template method using a 25 cm x 25 cm x 5 cm (depth) stainless steel template. This all soil samples were crushed into a powder form to reduce the particle size to get some form of homogeneity and sieved through a 2 mm mesh sieve to remove all undesirable particle size. They were then dried in an oven at 105 °C for 24 h (Salama et al., 2015). Soil samples were sealed in gas-tight polyethylene containers (Marinelli beakers), tightly closed, and stored for four weeks to allow radioactive equilibrium. The geometric efficiency of soil matrices within the containers was calibrated the IAEA-326 reference soil material (International Atomic Energy Agency, Vienna, Austria), which was spiked with a series of radionuclides (40K, 90Sr, 210Pb, 226Ra, 228Ra, 228Th, ²³⁰Th, ²³²Th, ²³⁴U, ²³⁸U, ²³⁸Pu, and ²³⁹+²⁴⁰Pu), having a total recommended activity of 886.619 Bq/kg (dry weight) as of December 31, 1994. Gamma-ray measurements were performed using an HPGe gamma-spectrometer with 40% efficiency in the laboratories of the Nuclear Martial Authority, Egypt. And 2.0 keV energy resolution at the 1.33 MeV photons of 60Co, shielded by 4 mm Pb, 1 mm Cd, and 1 mm Cu. Spectral analysis was carried out with the Maestro software. The specific activities of ²²⁶Ra and ²³²Th were derived from their progeny radionuclides ²¹⁴Bi (609 keV) and ²²⁸Ac (911 keV), respectively, while 40K activity was determined from its 1460 keV γ -line. The average counting time for all samples was approximately 72,000 seconds.

The results revealed that the distribution of ²²⁶Ra, ²³²Th, and ⁴⁰K in soil is spatially heterogeneous Therefore, comparing the radiological effects from the soil samples containing different amounts of 226Ra, 232Th and 40K can be obtained by computing a common index called the radium equivalent activity (Raeq) in Bq/kg. It is calculated using the following relation (Beretka, &. Mathew, 1985):

Raeq=CRa + 1.43CTh + 0.07CK.....(1)Where, CRa,CTh and CKare the activity concentrations (Bq/kg) of 226Ra, 232Th 40Krespectively. While defining Raeq activity according to Eq. (1), it has been assumed that 370 Bq/kg of226Ra or 259 Bq/ kg of 232Th or 4810Bq /kg of 40K produce the same gamma dose rate. The external gamma absorbed dose rate in the air at 1 m above ground level is calculated from the measured activities of 226Ra, 232Th and 40K in soil assuming that the other radionuclides, such as 137Cs,90Sr and the 235U series can be neglected as they contribute very little to the total dose from environmental background (Kocher & Sjoreen, 1985) and (Jacob., et al. 1986). Calculations were performed according to the following equation (UNSCEAR 2000):

D (nGyh-1) = 0.427CRa + 0.662CTh + 0.0432CK...... (2) Where D is the dose rate in nGy/h and CRa, CTh and CKare the specific activities (Bq/kg) of 226Ra, 232Th and 40K, respectively. In the above equation, it is assumed that all decay products of 226Ra and232Th are in radioactive equilibrium with their precursors. The external hazard index (Hex) is defined as (Beretka, & Mathew, 1985):

Hex = CRa/370 + CTh/259 + CK/4810... (3) Where, CRa, CTh and CKare the specific activities (Bq/kg) of 226Ra, 232Th and 40K, respectively. The value of this index must be less than unity in order to keep the radiation hazard insignificant. The maximum value of Hex equal to unity corresponds to the upper radium equivalent activity (370Bq/kg).Considering 0.7 Sv/Gy conversion coefficient from the absorbed dose in air to the effective dose and the indoor occupancy factor 0.2 (people on the average, spent 20% of their time outdoors) (UNSCEAR., 2000), the annual effective doses are calculated: Annual effective dose

$$(Sv/y) = D (Gy) \times 24(h) \times 365(d) \times 0.7 \times 0.2...$$
 (4)

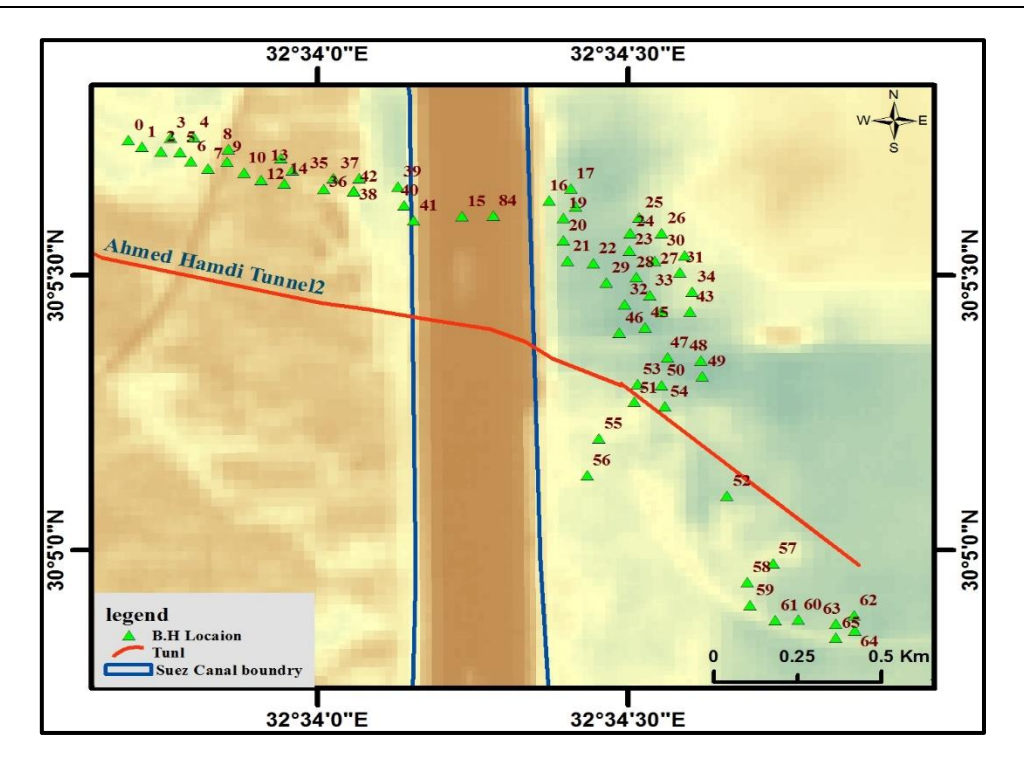


Fig. 3. Borehole locations map of the study area.

4. 1.2. Airborne Radiometric Data Analysis

This part is based on the interpretation of airborne gamma-ray spectrometric maps, where radiometric data were extracted, , and used to construct detailed radiometric distribution maps for the study area. Airborne gamma-ray spectrometry is a geophysical technique widely applied to detect and map the distribution of natural radioelements such as uranium, thorium, and potassium on regional scale. The method is based on measuring gamma radiation emitted from rocks and soils using detectors installed on aircrafts, allowing rapid, cost-effective, and continuous data acquisition. The processed airborne data are then used to construct radiometric maps that are highly valuable for geological mapping, mineral exploration, and environmental monitoring.

Thus, gamma-ray spectrometric data could be used to detect areas of consistent lithology and contact between different lithologies (Atef et. al., 2000). The surface concentrations of the radioelement (i.e., potassium,

Uranium and thorium) can be quantified by measuring the intensities of the gamma radiation emitted by K Bi214 and Tl208 radioisotopes respectively. These measurements can then be correlated with surface concentrations using suitable calibration processes (Grasty et al., 1985). The information gathered is then utilized to create maps illustrating the distribution of the three radioelements which is of great help in

determining the radioactive levels in the study area and their relation with the surface radioactive levels. The airborne gamma ray radiometric survey of Suez area and surroundings was carried out by Aero-Service Division, Western Geophysical Company of America on 1982 (Aero Service Report, 1984) for the Egyptian General Petroleum Corporation (EGPC) and the Egyptian Geological Survey and Mining Authority (EGSMA). The radiometric data are gridded to generate total count (TC in μ R/h), equivalent uranium (eU in ppm), equivalent thorium (eTh in ppm) and potassium (K in %) maps which display the surface distribution of these elements and clearly delineate surface lineaments.

5. Results and discussion

The spectrometric maps of the Suez area and its surroundings were processed and interpreted in relation to the prevailing geological rock units to evaluate the radiological hazards within the study area and to distinguish between safe and unsafe sites for workers and inhabitants. The radiological assessment was conducted through several parameters, including exposure rate, effective dose rate (EDR), internal and external hazard indices (Hin and Hex), in addition to determination of the specific activity concentrations of 238U, 226Ra, 232Th, and 40K in the collected samples.

For ²³⁸U, the specific activity concentrations (Bq/kg) ranged from (22 - 153), with a mean value of 87.5,

232Th (5.87-45.47) with average25.67, and 40K (380-566.5) with average 473 at the surface level (0 m), as shown in (Table 1) and (Fig. 4). At a depth of 5 m, the ²³⁸ U concentrations (Bq/kg) ranged from (17 -151.90), with a mean value of 84.45, 232Th (4.87-49.53) with average 27, and 40K (381-566) with average 473, as shown in (Table 1) and (Fig. 5). At a depth of 10 m, the 238 U concentrations (Bq/kg) ranged from (12.35 - 148), with an average of 80, 232Th (4-52.78) with average 28.39, and 40K (382-566.6) with average 474, as illustrated in (Table 1) and (Fig. 6). On the other hand, the airborne spectrometric measurements showed relatively higher concentrations, the 238U ranged from 70 to 490 with average 280, 232Th (8-173) with average 90, and 40K (185–970) with average 580 as shown in (Fig. 7).

The calculated radiological parameters indicate that the exposure rate and the effective dose rate (EDR) for most of the ground samples lie within the recommended safe limits. Similarly, the internal (Hin) and external (Hex) hazard indices were found to be less than unity in most of the studied sites, suggesting acceptable radiological conditions (Tables 2 to 4) and (Figs. 8 to 15). However, the airborne measurements recorded relatively elevated values compared to the ground samples, in some cases exceeding the worldwide averages, highlighting the importance of continuous monitoring and the application of appropriate radiological precautions in the study area (Figs. 16 to 18).

Table 1. The activity concentrations 238U, 232Th and 40K in Suez area soil at depths (0.00, 5.00, and 10.00) m.

)) m.	0.0\			00)			0.00	
Sample	Depth (0.	.00)		Depth (5	.00)		Depth (10.00)		
NO.	²³⁸ U	²³² Th	⁴⁰ K	²³⁸ U	²³² Th	⁴⁰ K	²³⁸ U ²³² Th		⁴⁰ K
				_	(Bq/k)g			(Bq/k)g	(Bq/kg)
1-1	(Bq/kg) 64.22	(Bq/k) g 35.32	(Bq/kg) 416.29	(Bq/kg) 17.29	45.06	(Bq/kg) 416.29	(Bq/kg) 37.05	12.18	400.64
2-1	22.23	25.17	532.1	39.52	25.98	456.98	123.5	24.36	469.5
4-1	40.755	15.83	500.8	75.33	33.29	519.58	12.35	16.24	519.58
6-1	91.39	6.90	485.15	96.33	13.80	400.64	86.45	12.18	566.53
		10.15			1	532.1	74.1		
10-1	56.81		503.93	48.16 125.97	8.53 4.87	538.36	24.7	36.54	503.93
12-1	35.815	13.80	538.36					4.06	538.36
13-1	92.625	21.52	469.5	90.15	45.06	469.5	49.4	44.66	406.9
15-1	137.085	25.17	400.64	64.22	6.09	400.64	61.75	9.2	400.64
17-1	132.145	45.47	406.9	23.46	29.23	416.29	74.1	52.78	416.29
20-1	116.09	31.66	416.29	83.98	9.39	519.58	86.45	40.6	519.58
22-1	46.93	19.08	550.88	97.56	14.61	469.5	98.8	28.42	469.5
25-1	69.16	15.83	450.72	27.17	28.82	450.72	37.05	12.18	400.64
26-1	97.565	34.10	397.51	45.69	34.10	397.51	111.15	32.48	381.86
28-1	109.915	10.96	519.58	116.09	21.51	550.88	49.4	9.2	550.88
30-1	116.09	7.308	510.19	80.27	37.35	510.19	74.1	4.06	510.19
31-1	125.97	5.87	541.49	19.76	5.846	541.49	98.8	16.24	532.1
33-1	137.085	9.46	428.81	114.85	17.86	428.81	12.35	36.54	428.81
36-1	69.16	29.31	416.29	67.92	34.10	416.29	24.7	32.48	416.29
38-1	23.465	15.83	400.64	125.97	15.83	566.53	123.5	9.2	466.37
41-1	35.815	41.04	456.98	108.68	27.60	456.98	135.85	16.24	456.98
42-1	58.045	15.02	566.53	137.08	45.06	566.53	49.4	9.2	469.5
44-1	81.51	11.39	519.58	56.81	37.35	485.15	148.2	40.6	532.1
46-1	153.14	7.308	466.37	151.90	19.89	466.37	24.7	24.36	466.37
48-1	97.565	19.89	380.2	108.68	5.602	381.86	123.5	4.06	541.49
50-1	46.93	34.104	403.77	116.09	49.53	532.1	98.8	12.18	566.53
53-1	32.11	36.54	532.1	93.86	38.97	406.9	123.5	12.18	566.53
55-1	117.325	32.48	469.5	22.23	21.92	469.5	61.75	9.2	450.72
56-1	100.035	40.6	510.19	58.04	14.61	510.19	12.35	52.78	416.29
58-1	27.17	16.24	456.98	65.45	8.93	503.93	49.4	52.78	566.53
60-1	23.465	44.6	566.53	82.74	15.02	403.77	111.15	9.2	406.9
Minimum	22.23	5.87	380.2	17.29	4.87	381.8	12.35	4.02	381.8
Maximum	153.14	45.47	566.5	151.9	49.53	566.5	148	52.78	566.6
Average	87.68	25.67	473	84.45	27	473	80	28.39	474.3

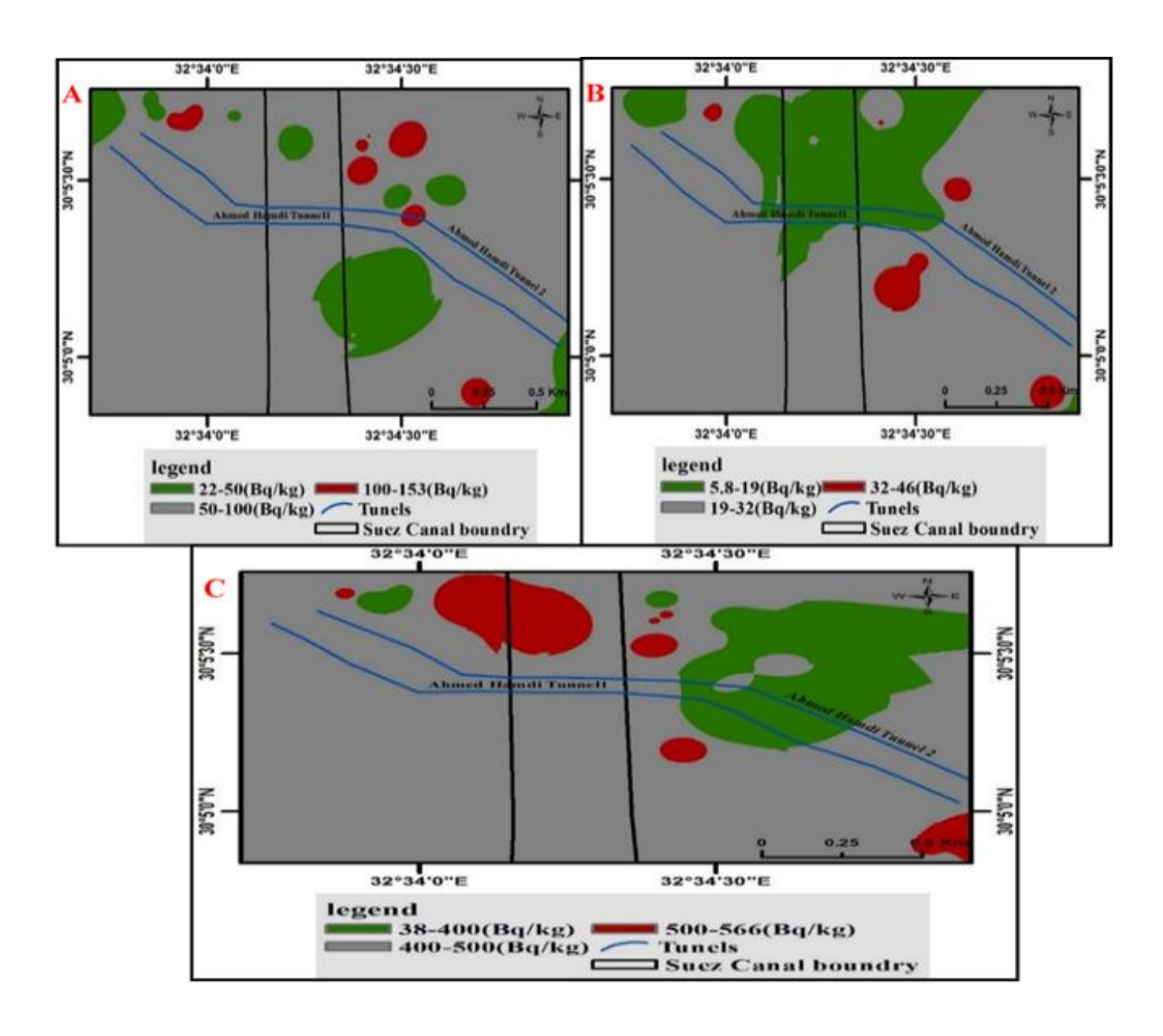


Fig. 4. Spatial distribution maps of the activity concentrations of gamma radiation elements; uranium (A), thorium (B), and potassium (C) at (0 m depth) within the study area.

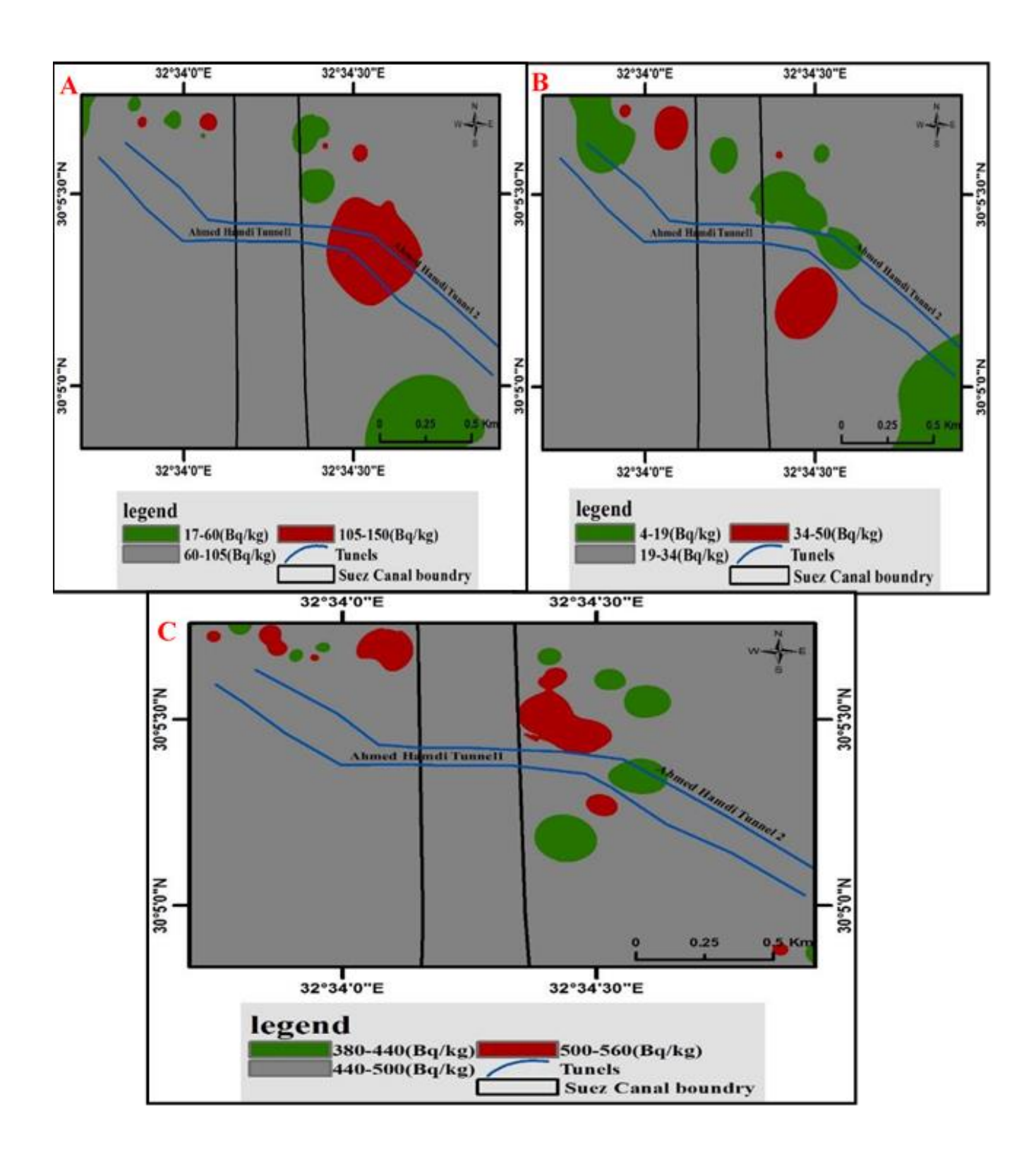


Fig. 5. Spatial distribution maps of the activity concentrations of gamma radiation elements; uranium (A), thorium (B), and potassium (C) at (5 m depth) within the study area.

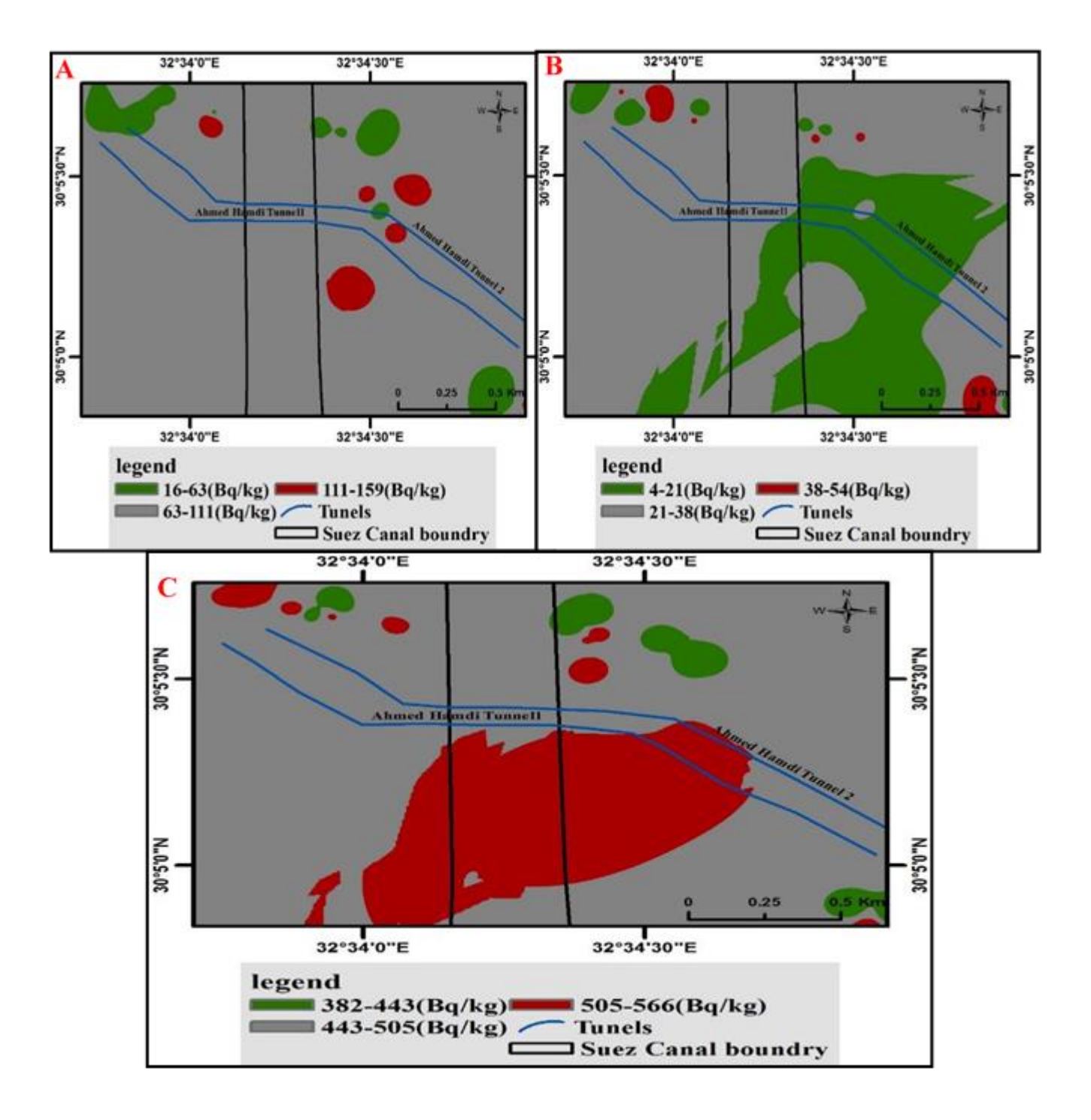


Fig. 6. Spatial distribution maps of the activity concentrations of gamma radiation elements; uranium (A), thorium (B), and potassium (C) at (10 m depth) within the study area.

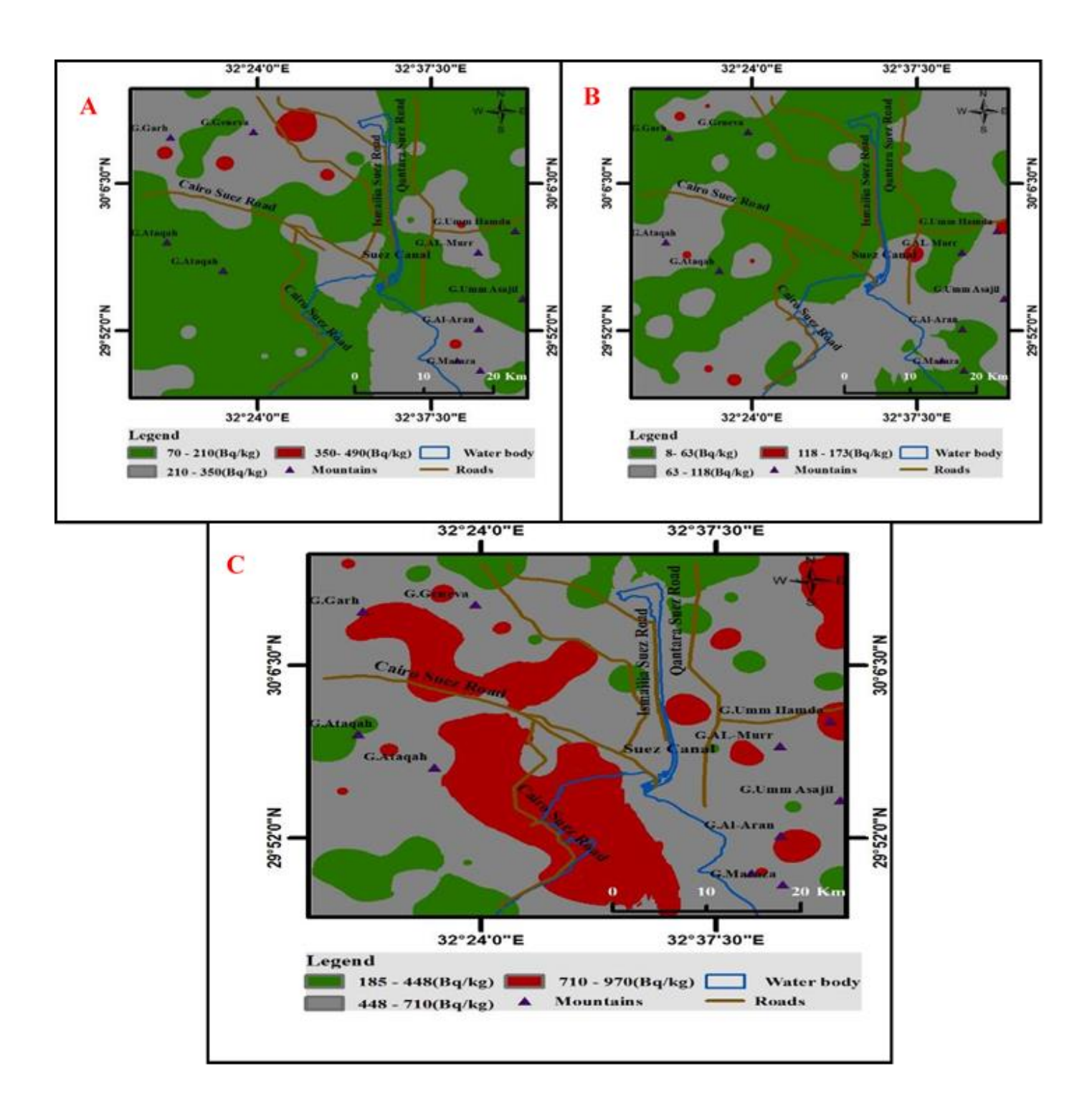


Fig. 7. Spatial distribution airborne maps of the activity concentrations of gamma radiation elements; uranium (A), thorium (B), and potassium (C) at the study area.

Table 2. The R_{aeq} , external Hazard index (Hex), internal hazards, Gamma index level, internal level index, Absorbed gamma dose rate, and Annual effective dose equivalent (in- and outdoor) for Suez area soil samples at (0.00) m depth.

Sample NO.	R _{eq} (Bq/Kg)	Hex _(Bq/Kg)		Internal Hazerd	Gamma Index	H _{in}	D _{y (nGy/h)}	D _{annual} (mSv/Y)	
		Without	With					(Indoor)	(outdoor)
4.4	1.46.70	window	window	0.57	0.52	0.22	60.06	0.24	0.00
1-1	146.78	0.37	0.19	0.57	0.53	0.32	68.96	0.34	0.08
2-1	99.19	0.25	0.13	0.32	0.37	0.11	48.09	0.23	0.06
4-1	101.95	0.26	0.13	0.38	0.38	0.20	49.54	0.24	0.06
6-1	138.61	0.37	0.18	0.62	0.50	0.45	66.74	0.33	0.08
10-1	110.12	0.29	0.14	0.45	0.40	0.28	53.56	0.26	0.06
12-1	97.08	0.25	0.13	0.35	0.38	0.18	47.57	0.23	0.06
13-1	159.54	0.42	0.21	0.68	0.57	0.46	75.73	0.37	0.09
15-1	203.93	0.53	0.27	0.92	0.71	0.68	95.67	0.47	0.12
17-1	228.50	0.59	0.30	0.97	0.80	0.66	106.25	0.52	0.13
20-1	193.42	0.50	0.26	0.83	0.68	0.58	90.69	0.44	0.11
22-1	116.63	0.30	0.15	0.44	0.43	0.23	56.50	0.27	0.07
25-1	126.50	0.30	0.17	0.52	0.46	0.34	60.57	0.29	0.07
26-1	176.94	0.46	0.23	0.74	0.63	0.48	82.83	0.41	0.10
28-1	165.59	0.44	0.22	0.74	0.59	0.55	79.25	0.39	0.09
30-1	165.82	0.44	0.22	0.76	0.59	0.58	79.44	0.39	0.09
31-1	176.02	0.47	0.23	0.81	0.63	0.62	84.41	0.41	0.10
33-1	183.63	0.49	0.24	0.86	0.65	0.68	87.09	0.42	0.1
36-1	143.13	0.37	0.19	0.57	0.51	0.34	67.51	0.33	0.08
38-1	76.95	0.20	0.10	0.27	0.29	0.11	37.38	0.18	0.04
41-1	129.69	0.33	0.17	0.44	0.47	0.17	61.09	0.30	0.07
42-1	123.14	0.32	0.16	0.48	0.45	0.29	59.77	0.29	0.07
44-1	137.77	0.36	0.18	0.59	0.50	0.40	66.38	0.32	0.08
46-1	199.50	0.53	0.26	0.95	0.70	0.76	94.74	0.46	0.11
48-1	155.41	0.41	0.20	0.68	0.55	0.48	73.35	0.36	0.09
50-1	126.78	0.32	0.17	0.46	0.46	0.23	59.69	0.29	0.07
53-1	126.49	0.32	0.17	0.42	0.47	0.16	60.22	0.29	0.07
55-1	191.21	0.50	0.25	0.83	0.68	0.58	90.17	0.44	0.11
56-1	203.18	0.52	0.27	0.81	0.73	0.50	95.22	0.46	0.12
58-1	85.08	0.22	0.11	0.30	0.32	0.13	41.44	0.20	0.05
60-1	83.92	0.22	0.113	0.29	0.32	0.11	41.77	0.20	0.05
Minimum	76.95	0.22	0.10	0.27	0.29	0.11	37.38	0.18	0.05
Maximum	228.50	0.59	0.30	0.97	0.80	0.68	106.2	0.52	0.13
Average	152.4	0.40	0.20	0.62	0.54	0.39	0.71.8	0.35	0.09

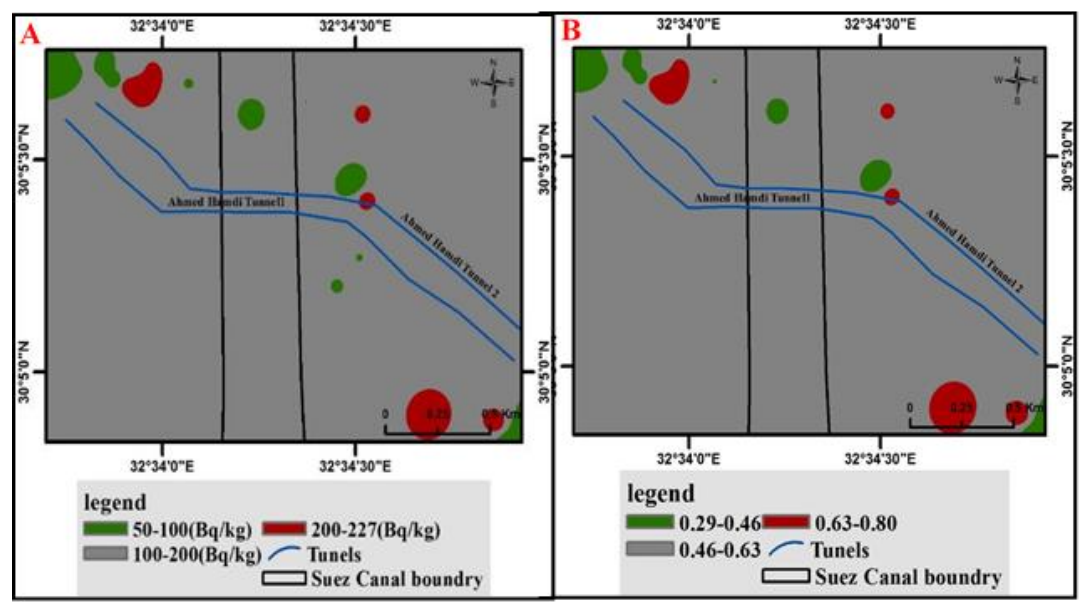


Fig. 8. The activity distribution map of the Radium equivalent (A) and Gamma index level (B) in the study area.

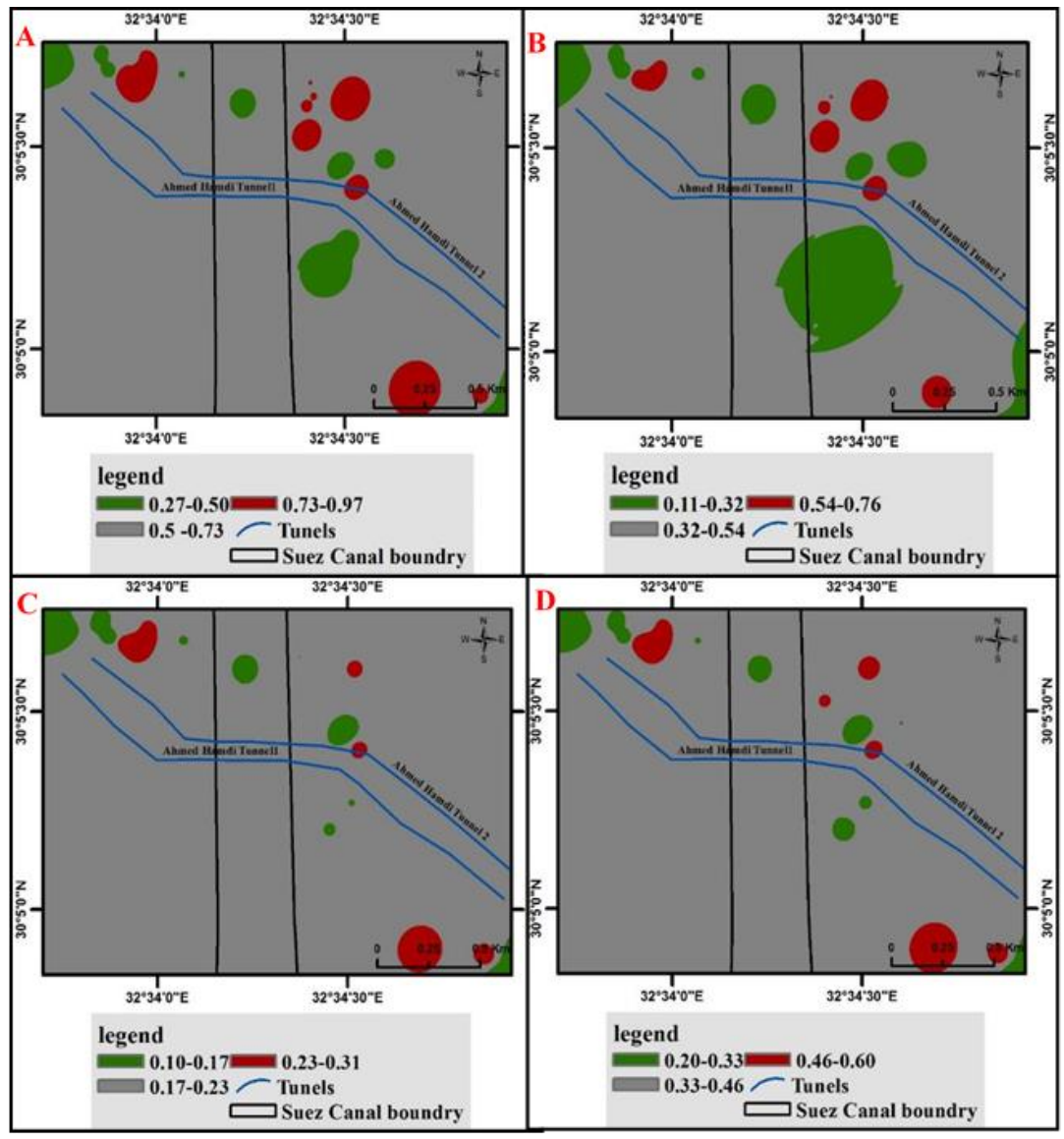


Fig. 9. The activity distribution map of the internal hazards (A), internal level index (alpha) (B), External hazards (without windows) (C) and (with windows) (D) in the study area.

Table 3. The R_{aeq} , external Hazard index (Hex), internal hazards, Gamma index level, internal level index, Absorbed gamma dose rate, and Annual effective dose equivalent (in- and outdoor) for Suez area soil samples at (5.00) m depth.

Sample	R _{eq} Hex (Bq/Kg)		Internal	Internal Gamma		$\mathbf{D}_{\mathbf{y}}$	D _{annual}		
NO.	(Bq/Kg)			Hazerd	Index		(nGy/h)	(mSv/Y)	
		Without	With					(Indoor)	(outdoor)
		window	window						
1-1	113.78	0.28	0.15	0.35	0.42	0.08	53.33	0.261	0.065
2-1	111.86	0.29	0.15	0.41	0.41	0.19	53.45	0.262	0.065
4-1	162.95	0.42	0.22	0.64	0.59	0.37	77.14	0.378	0.094
6-1	146.91	0.39	0.19	0.65	0.52	0.48	69.78	0.342	0.085
10-1	101.32	0.26	0.13	0.40	0.38	0.24	49.73	0.244	0.061
12-1	174.39	0.46	0.23	0.81	0.62	0.62	83.67	0.410	0.102
13-1	190.75	0.49	0.25	0.75	0.68	0.45	89.21	0.437	0.109
15-1	103.77	0.27	0.14	0.45	0.37	0.32	50.15	0.246	0.061
17-1	97.321	0.24	0.13	0.32	0.36	0.11	46.35	0.227	0.056
20-1	137.34	0.36	0.18	0.59	0.50	0.41	66.26	0.325	0.081
22-1	154.61	0.41	0.20	0.68	0.55	0.48	73.72	0.361	0.090
25-1	103.09	0.26	0.14	0.35	0.38	0.13	49.24	0.241	0.060
26-1	125.07	0.32	0.17	0.46	0.45	0.22	58.86	0.288	0.072
28-1	189.27	0.50	0.25	0.82	0.67	0.58	89.96	0.441	0.110
30-1	172.97	0.45	0.23	0.68	0.62	0.40	81.55	0.403	0.109
31-1	69.815	0.18	0.09	0.24	0.27	0.09	35.33	0.173	0.043
33-1	173.41	0.46	0.23	0.77	0.61	0.57	82.03	0.402	0.106
36-1	148.74	0.38	0.20	0.58	0.53	0.34	69.91	0.343	0.085
38-1	192.23	0.51	0.25	0.85	0.68	0.62	91.65	0.449	0.112
41-1	183.34	0.48	0.24	0.79	0.65	0.54	86.41	0.424	0.106
42-1	245.15	0.64	0.33	1.03	0.87	0.68	114.9	0.564	0.141
44-1	147.57	0.38	0.19	0.55	0.53	0.28	69.67	0.342	0.085
46-1	216.26	0.57	0.29	0.99	0.76	0.76	101.9	0.506	0.125
48-1	146.09	0.39	0.19	0.68	0.52	0.54	69.61	0.341	0.085
50-1	227.89	0.59	0.307	0.92	0.81	0.58	106.6	0.523	0.130
53-1	180.92	0.47	0.24	0.74	0.64	0.46	84.53	0.414	0.103
55-1	89.732	0.23	0.12	0.30	0.34	0.11	43.46	0.213	0.053
56-1	118.23	0.31	0.15	0.47	0.43	0.29	57.16	0.280	0.070
58-1	117.03	0.31	0.15	0.49	0.43	0.32	56.80	0.278	0.069
60-1	135.31	0.35	0.18	0.58	0.48	0.41	64.39	0.316	0.079
Minimum	245.18	0.18	0.09	0.30	0.27	0.08	35.33	0.173	0.043
Maximum	69.81	0.64	0.33	1.03	0.87	0.76	114.9	0.523	0.141
Average	157.5	0.41	0.21	0.66	0.57	0.42	75.11	0.348	0.092

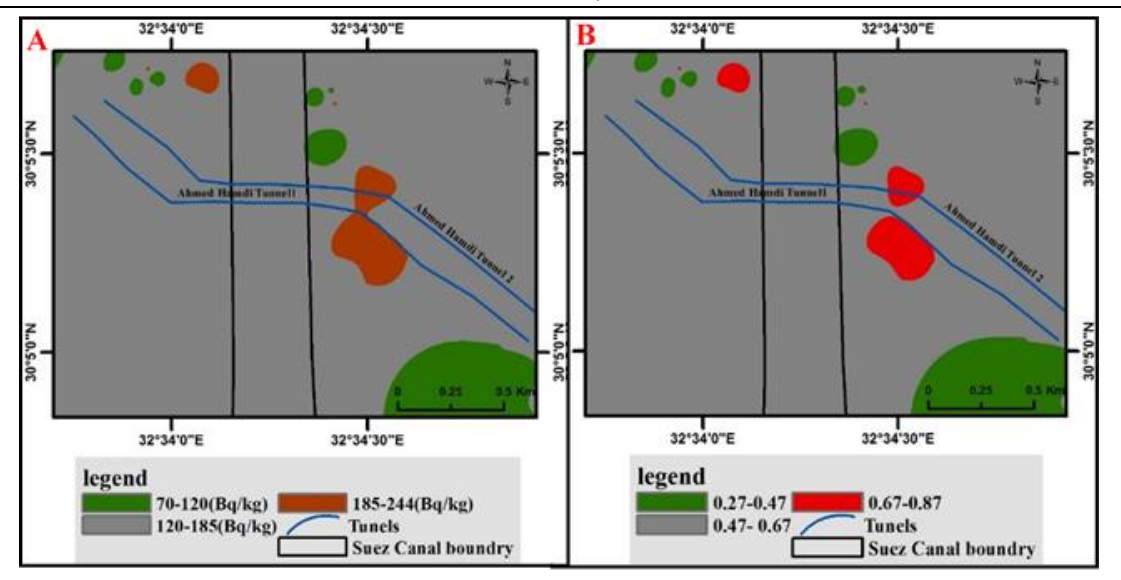


Fig. 10. The activity distribution map of the Radium equivalent (A) and Gamma index level (B) in the study area.

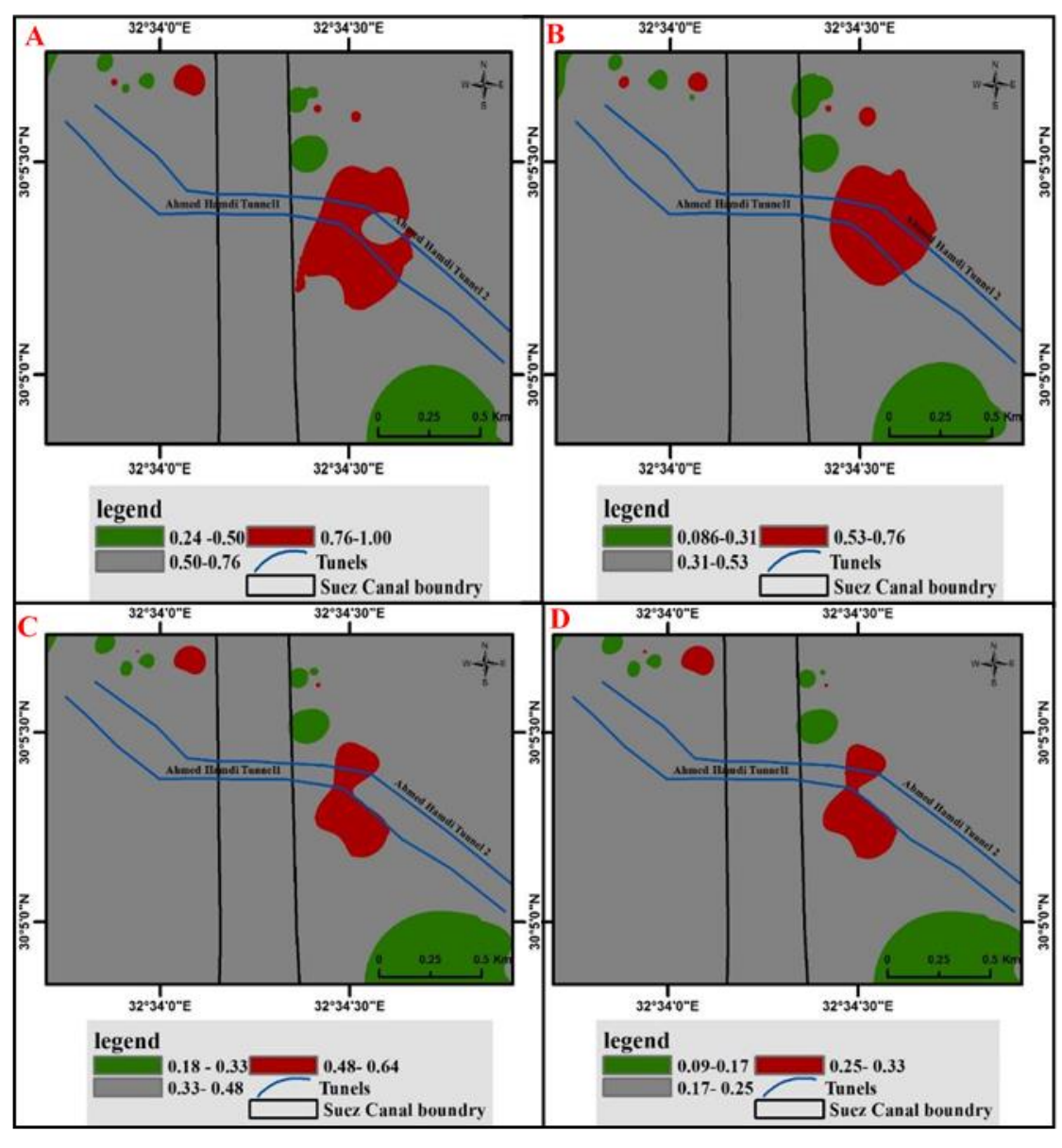


Fig. 11. The activity distribution map of the internal hazards (A), internal level index (alpha) (B) External hazards (without windows) (C) and (with windows) (D) in the study area.

Egypt. J. Geo. Vol. 69 (2025)

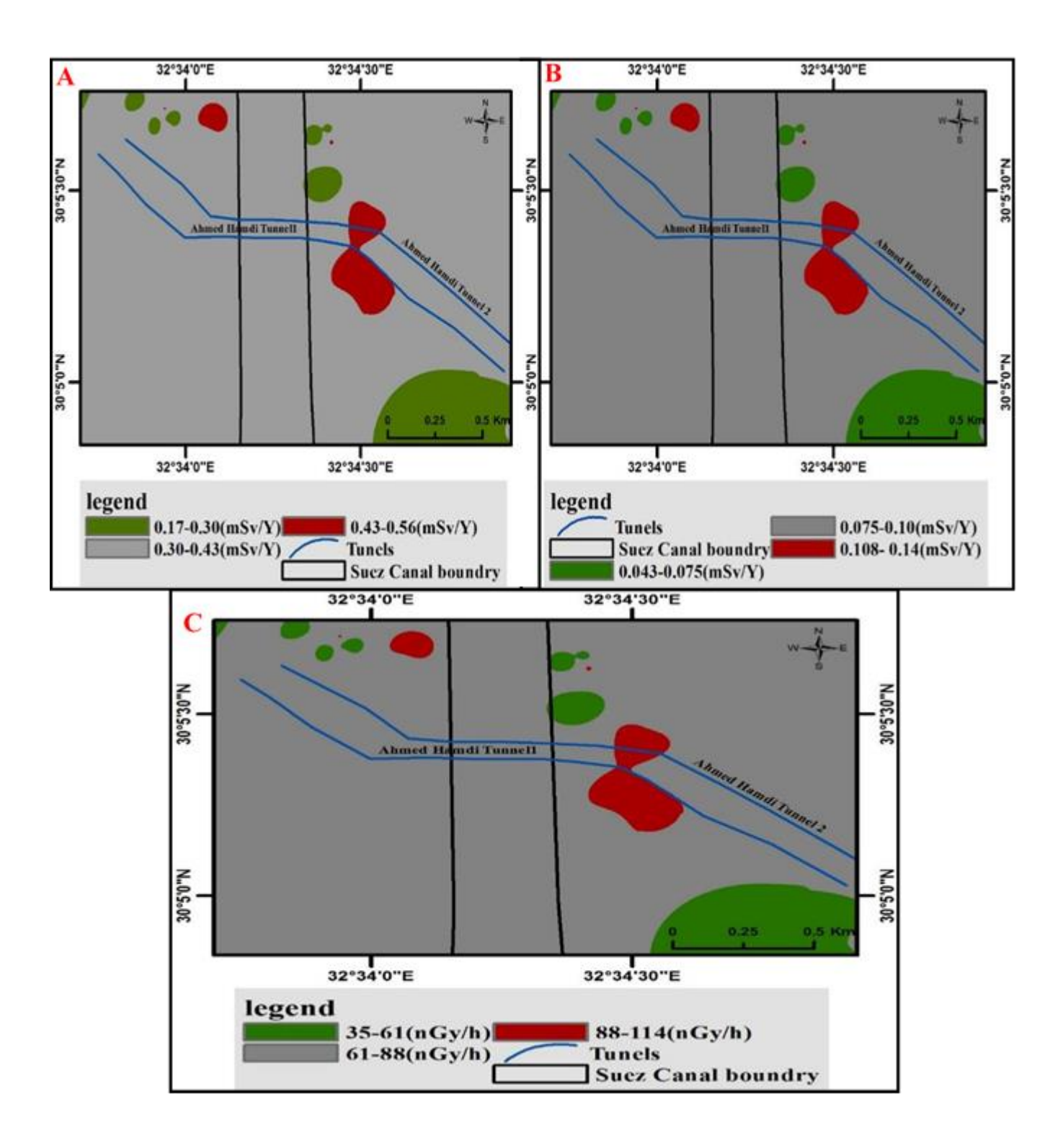


Fig. 12. The activity distribution map of the Annual effective dose equivalent (indoor) (A), (outdoor) (B) and absorbed dose rate (C) in the study area.

Table 4. The R_{aeq} , external Hazard index (Hex), internal hazards, Gamma index level, internal level index, Absorbed gamma dose rate, and Annual effective dose equivalent (in- and outdoor) for Suez area soil samples at (10.00)m depth.

Sample NO.	R _{eq} (Bq/Kg)	Hex (Bq/Kg)		Internal	Gamma	н	$\mathbf{D_{v}}$	D _{annual} (mSv/Y)	
	(-18)	Without window	With window	Hazard	Index	H _{in}	(nGy/h)	(Indoor)	(outdoor)
1-1	99.97	0.26	0.135	0.37	0.36	0.19	47.82	0.23	0.06
2-1	201.74	0.53	0.27	0.89	0.71	0.64	95.05	0.46	0.11
4-1	84.15	0.22	0.11	0.28	0.32	0.09	41.38	0.20	0.05
6-1	153.01	0.41	0.20	0.66	0.55	0.45	73.66	0.36	0.09
10-1	171.68	0.44	0.23	0.67	0.62	0.38	80.84	0.39	0.09
12-1	76.24	0.20	0.10	0.28	0.29	0.14	38.34	0.18	0.04
13-1	147.5	0.37	0.19	0.53	0.53	0.25	68.85	0.34	0.08
15-1	111.97	0.29	0.15	0.47	0.40	0.32	53.75	0.26	0.06
17-1	187.00	0.47	0.25	0.71	0.66	0.38	86.77	0.42	0.10
20-1	187.49	0.48	0.25	0.74	0.67	0.43	88.14	0.43	0.11
22-1	185.83	0.48	0.26	0.78	0.66	0.52	87.49	0.43	0.11
25-1	93.08	0.24	0.12	0.36	0.34	0.20	44.86	0.22	0.05
26-1	188.16	0.49	0.26	0.80	0.66	0.55	87.94	0.43	0.11
28-1	113.59	0.30	0.15	0.45	0.42	0.27	55.38	0.27	0.07
30-1	176.59	0.45	0.23	0.67	0.63	0.36	82.92	0.41	0.10
31-1	159.36	0.42	0.21	0.69	0.57	0.48	76.27	0.37	0.09
33-1	105.38	0.26	0.14	0.32	0.39	0.08	49.75	0.24	0.06
36-1	160.16	0.42	0.21	0.68	0.57	0.46	75.59	0.37	0.09
38-1	180.02	0.48	0.24	0.83	0.63	0.64	85.59	0.42	0.10
41-1	206.38	0.54	0.28	0.94	0.72	0.72	97.41	0.47	0.11
42-1	108.20	0.28	0.14	0.45	0.39	0.29	52.51	0.27	0.06
44-1	258.34	0.67	0.34	1.12	0.91	0.79	121.0	0.59	0.14
46-1	106.33	0.27	0.14	0.37	0.39	0.16	50.92	0.24	0.06
48-1	176.22	0.47	0.23	0.81	0.63	0.61	84.42	0.41	0.10
50-1	168.41	0.44	0.22	0.74	0.60	0.53	80.76	0.39	0.10
53-1	206.60	0.54	0.27	0.89	0.73	0.61	97.82	0.48	0.12
55-1	120.77	0.32	0.16	0.51	0.43	0.35	58.12	0.28	0.07
56-1	126.48	0.31	0.17	0.38	0.46	0.08	58.81	0.28	0.07
58-1	186.24	0.48	0.25	0.73	0.67	0.41	87.88	0.43	0.11
60-1	161.57	0.43	0.22	0.76	0.57	0.59	76.85	0.37	0.09
Minimum	76.24	0.22	0.10	0.28	0.32	0.08	38.34	0.18	0.04
Maximum	258.34	0.54	0.34	1.12	0.91	0.72	121	0.59	0.14
Average	167.29	0.38	0.22	0.70	0.61	0.4	79.67	0.38	0.09

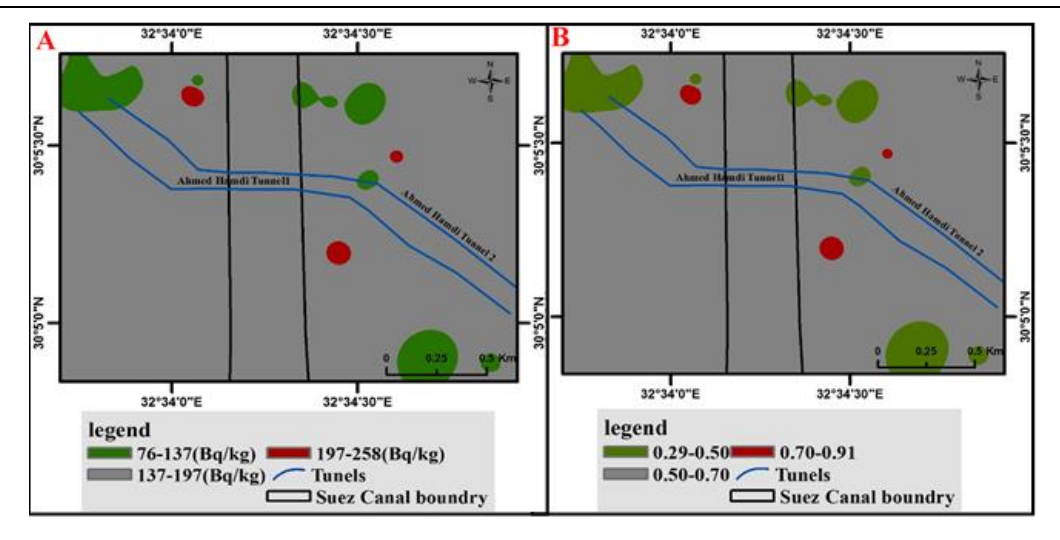


Fig. 13. The activity distribution map of the Radium equivalent (A) and Gamma index level (B) in the study area.

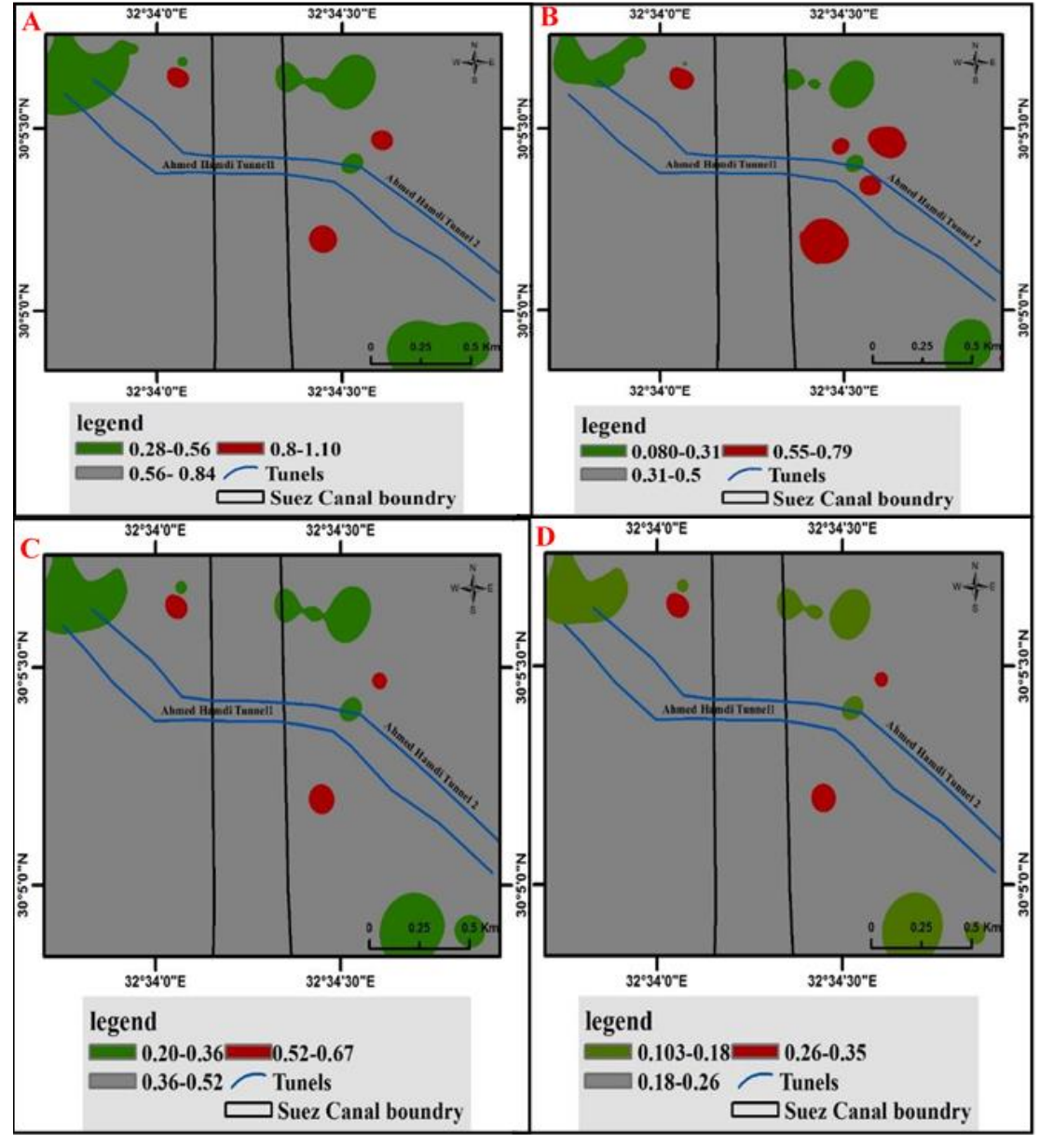


Fig. 14. The activity distribution map of the internal hazards (A), internal level index (alpha) (B) External hazards (without windows) (C) and (with windows) (D) in the study area.

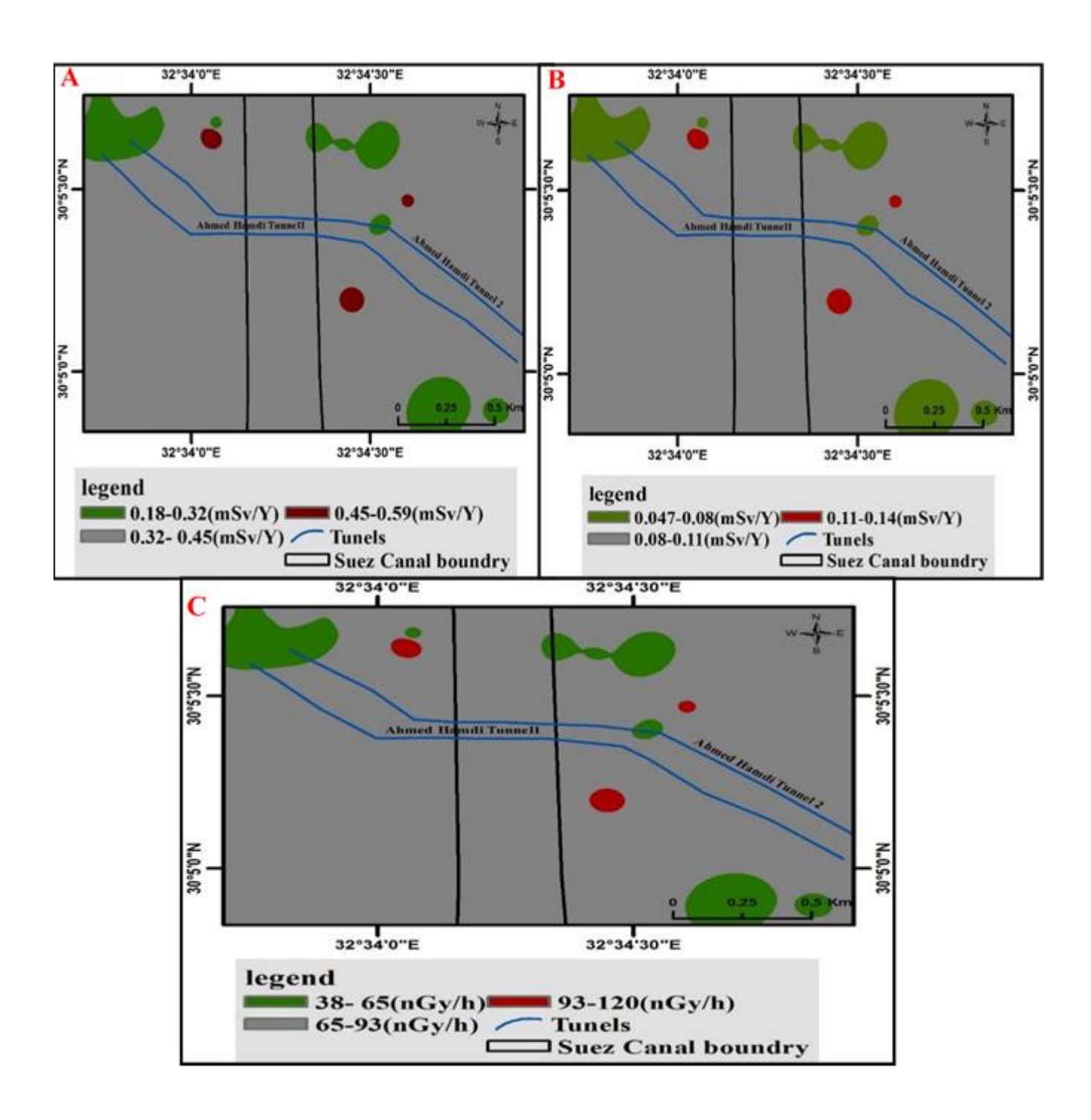


Fig. 15. The activity distribution map of the Annual effective dose equivalent (indoor) (A), (outdoor) (B) and absorbed dose rate (C) in the study area.

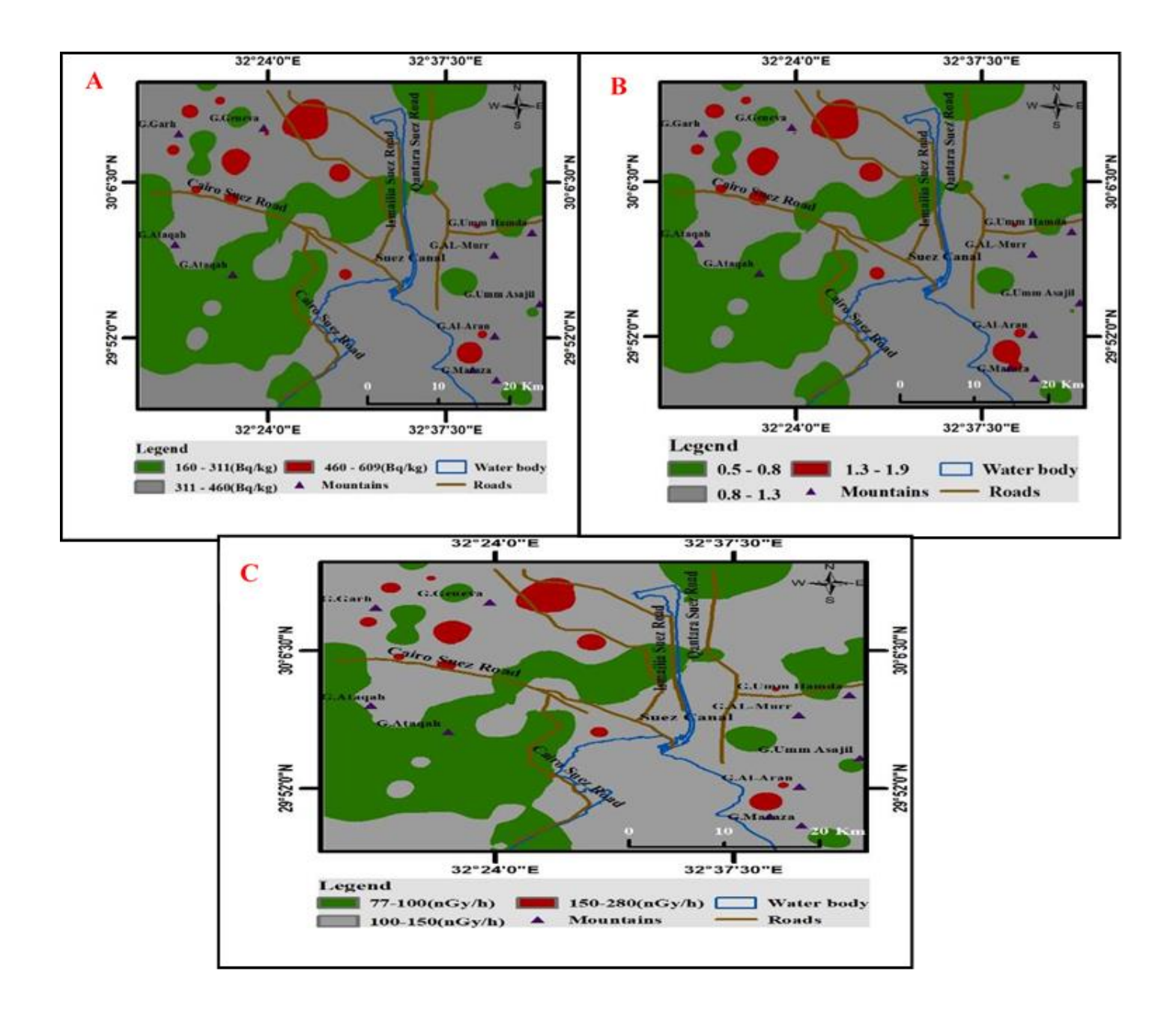


Fig. 16. The activity distribution airborne map of the Radium equivalent (A), Gamma index level (B) and absorbed dose rate (C) in the study area.

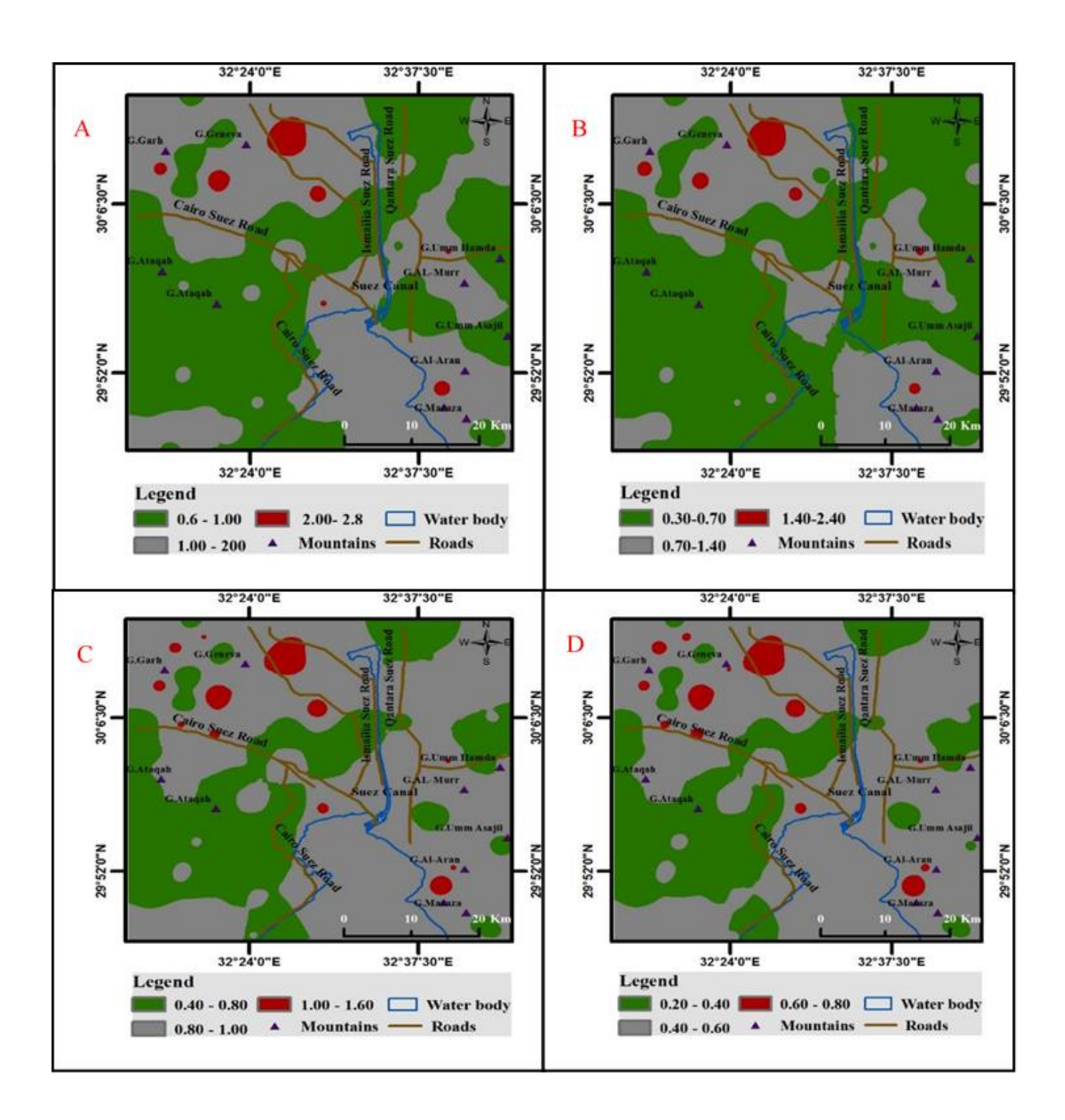


Fig. 17. The activity distribution airborne map of the internal hazards (A), internal level index (alpha) (B) External hazards (without windows) (C) and (with windows) (D) in the study area.

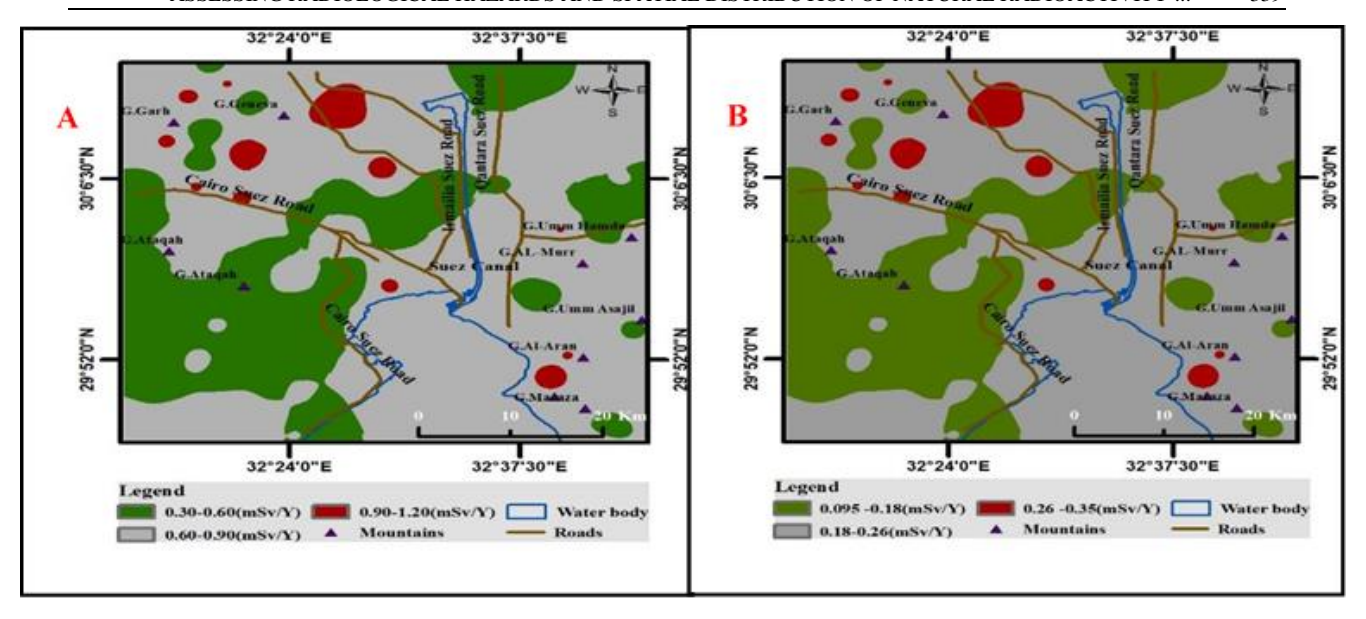


Fig. 18. The activity distribution airborne map of the Annual effective Dose equivalent (indoor) (A) and (outdoor) (B) in the study area.

6. Conclusions

Soil samples collected from the Suez area at different depths (surface 0 m, 5 m, and 10 m) in addition to airborne spectrometric measurements were analyzed for the specific activities of 238U, 232Th, and 40K. The measured radioactivity concentrations in the ground soil samples ranged between (12.3-153) Bq/kg for 238U (average ~82.6 Bq/kg), (4-53) Bq/kg for 232Th (average ~28.5 Bq/kg), and (380-566) Bq/kg for 40K (average ~470 Bq/kg). These values are generally consistent with the worldwide averages and fall within the reported ranges for Egyptian soils. In contrast, the airborne data showed relatively concentrations (70-490) Bq/kg for 238U, (8-173) Bq/kg for 232Th, and (185-970) Bq/kg for 40K, pointing to localized radiometric anomalies. The calculated average absorbed dose rate for the ground soil samples was about 72 nGy/h, which is slightly above the global average value of 59 nGy/h but still within safe limits. The corresponding average annual effective dose was estimated at 0.35 mSv/y, significantly lower than the recommended worldwide limit of 1 mSv/y for public exposure. The radium equivalent activity (Raeq) of the soil samples varied between 50 and 165 Bq/kg with an average of ~125 Bq/kg, which is well below the recommended safety limit of 370 Bq/kg. Similarly, the external hazard index (Hex) ranged from 0.27 to 0.97 (average ~0.62), remaining below unity and confirming that the studied soils are radiologically safe for human use. On the other hand, the airborne radiometric measurements exhibited absorbed dose rates (up to ~280 nGy/h) and increased Raeq values (up to ~609 Bq/kg), which in some cases approach or exceed the recommended international limits. This highlights the presence of localized radiological anomalies in the study area and underscores the need for continuous monitoring and further site-specific investigations.

7. Recommendations

Based on the obtained results, the following recommendations are suggested:

- 1. Continuous Monitoring: Areas showing elevated radiometric values in the airborne survey, particularly those with Raeq values approaching or exceeding international limits, should be subjected to continuous monitoring programs to ensure long-term radiological safety.
- 2. Detailed Geological Investigations: The localized anomalies should be further investigated through detailed geological and mineralogical studies to identify the lithological sources of elevated uranium, thorium, and potassium concentrations (e.g., heavy mineral-rich sands or phosphatebearing rocks).
- 3. Environmental and Public Health Considerations: Any future urban, industrial, or agricultural development in the Suez region should take into account the radiological background levels to minimize potential exposure risks to the public.
- 4. Future Research: It is recommended to integrate ground-based gamma-ray spectrometry and remote sensing techniques in future studies to achieve higher spatial resolution and improved interpretation of radiometric anomalies.

8. References

- A. Abdallah, M. Abdel Aal and M. Hussein., 1998.integrated Surf ace and Subsurface Structural Study of the Area be- tween Mediterranean and Eastern Desert, Egypt," EGPC's Exploration & Production Conference, Cairo, 1998, pp. 1-12.
- Abdallah MA, Abd El-Hady FM., 1966. Geology of Sadat area, Gulf of Suez. J Geol UAR 10(1):1–24.
- Abd El Rahman, R.M., Taalab, S.A., Al Full, Z.Z., Mohamed, M.S., Sayyed, M.I., Almousa, N., Hanfi, M.Y., 2022. Natural radionuclide levels and radiological hazards of Khour Abalea mineralized Pegmatites, Southeastern desert, Egypt. Minerals 12, 353.
- Abd-Elshafy, E., Abed, M.M., Shahat, W., 1989.
 Stratigraphic correlation andmacropaleontology of Akheider-Um Zeita Eocene successions. In: Gulf of SuezEgypt Proc. Symp. Phanerozoic & Development in Egypt. National Committeeof Geological Sciences & Al-Azhar University, pp. 79–106
- Abu El-Enain, F.M., Ali, M.M., Ismail, A.S., 1995. Petrography, geochemistry anddepositional history of the Eocene rocks in the area between northern Galalaand Gabal Ataqa, Western Gulf of Suez, Egypt. Ann. Geol. Surv. Egypt XX, 551–576.
- Aero-Service., 1984. Final operational report of airborne magnetic/radiation survey in the Eastern Desert, Egypt for the Egyptian General Petroleum Corporation. Aero-Service, Houston, Texas, April, 1984, Six Volumes.
- Arnous, M.O., 2004. Geo-environmental assessment of Cairo-Ismailia road area, Egypt, using remote sensing and geographic information system (GIS). Ph.D. Thesis, Geol.Dept., Fac. Sci., Suez Canal Univ, Ismailia, Egypt, 283p.
- Arnous MO, Mansour BMH., 2023. Utilizing multitemporal thermal data to assess environmental land degradation impacts: example from Suez Canal region Egypt. Environ Sci Pollut Res. https://doi.org/10.1007/s11356-022-22237-z.
- Arnous MO, Omar AE., 2018. Hydrometeorological hazards assessment of some basins in Southwestern Sinai area Egypt. J Coast Conserv 22:721–743. https://doi.org/10.1007/s11852-018-6604-2.
- Ambrosino, F., Thinov´a, L., Briestenský, M., Sabbarese, C., 2019. Analysis of Radon time series recorded in Slovak and Czech caves for the detection of anomalies due to seismic phenomens. Radiat. Protect. Dosim. 186 (2–3), 428–432.
- Ambrosino, F., Thinov'a, L., Briestenský, M., 'Sebela, S., Sabbarese, C., 2020a. Detecting time series anomalies using hybrid methods applied to Radon signals recorded in caves for possible correlation with earthquakes. Acta Geod. Geophys. 55 (3), 405–420.
- Atef, A. M., Sh, E. A. H., and Tamer, M. R., 2000. Uranium possibilities at El Gulf El Kiber area, Southwestern part of the Western Desert, Egypt. Prod. Conf., E.G.P.C., 22p.

- Ben-Avraham, Z., Ten Brink, U., & Bell, R., 1987.

 Morphology and structure of the northern Red Sea:
 Implications for the opening of the rift.
 Tectonophysics, 141(1–3), 229-247.
- Beretka, J., & Mathew, P. J., 1985. Natural radioactivity of Australian building materials, industrial wastes and by-products. Health Physics, 48(1), 87–95.
- Bignot, G., Strougo, A., 2002. Middle Eocene benthic foraminiferal assemblage's fromeastern Egypt, as biochronological and peritethyan lagoonal indicators. Rev.Micropaleontol., 73–98.
- Briestensky, M., Ambrosino, F., Smetanova, I., Thinova, L., Sebela, S., Stemberk, J., Pristasova, L., Pla, C., Benavente, D., 2022. Radon in Dead-end caves in Europe. J. Cave Karst Stud. 84 (2), 41–50.
- Bush P, Cooke RU, Burunsden D, Doornkamp JC, Jones DKC. 1980. Geology and geomorphology of the Suez city region, Egypt. J Arid Environ 3:265–281.
- Conoco. 1987. Geological map of Egypt, scale 1:500,000.Egyptian General Petroleum Corporation, Cairo, Egypt.
- Dangermond J., 1984. Review and synthesis of problems and directions for large scale geographic information system development. Proc
- D'Avino, V., Ambrosino, F., Bedogni, R., Campoy, A.I.C., La Verde, G., Vernetto, S., Vigorito, C.F., Pugliese, M., 2022. Characterization of Thermoluminescent Dosimeters for Neutron Dosimetry at High Altitudes. Sensors 22 (15), 5721.
- Effat, H. A. 2017. Mapping Potential Wind Energy Zones in Suez Canal Region, Using Satellite Data and Spatial Multicriteria Decision Models. Journal of Geoscience and Environment Protection, 5(10), 46–61.
- Egyptian Meteorological Authority (EMA). 1996. Climatic Atlas of Egypt. Cairo, Egypt
- Eke, B. C., Akomolafe, I. R., Ukewuihe, U. M., & Onyenegecha, C. P., 2024. Assessment of Radiation Hazard Indices Due to Natural Radionuclides in Soil Samples from Imo State University, Owerri, Nigeria. International Journal of Environmental Health Research.
- El Akkad S, Abdallah AM., 1971. Contribution to the geology of Gebel Ataqa area. Ann Geol Surv Egypt 1:21–42.
- EL-Shazly, E.M., M.A. Abdel hady, M. A. ELghawaby, I.A., EL-Kassas, A.B. Salman, AND M.A. Morsi.,1975. Geology and ground water potential of EL-Ismailia master plan study area. Remote Sensing Center. Academy of Scientific Research and Technology, Cairo, Egypt, pp.45.
- Forkapic, S., Vasin, J., Bikit, I., Mrdja, D., Bikit, K., Mili, S., 2017. Correlations between soil characteristics and radioactivity content of Vojvodina soil. J. Environ. Radioact. 166, 104–111.
- Gaafar, I., Hanfi, M., El-Ahll, L.S., Zeidan, I., 2021. Assessment of radiation hazards from phosphate

- rocks, Sibaiya area, central eastern desert, Egypt. Appl. Radiat. Isot. 173, 109734.
- Gargani, J., Moretti, I., & Letouzey, J., 2008. Evaporite accumulation during the Messinian Salinity Crisis: The Suez Rift case. Geophysical Research Letters, 35(2), L02401.
- Grastly R.L., Glynn J.E. and Grant J.A., 1985. The analysis of multichannel airborne gamma-ray spectra. Geophysics, 50: 2611–2620.
- Gupta AP., 1991. Remote sensing geology. Springer, Berlin, p 356 Hitesh B, Vikas R, Gurtej SS., 2016 Effect of waste marble powder on UCS and free swell index of clayey soil. Int J Sci Res Educ 4(8):5657– 5663.
- IAEA Annual Report 2007.IAEA Safety Standards Categorization of Radioactive Sources, USA.
- Jakhu, R., Mehra, R., Bangotra, P., Kaur, K., Mittal, H.M., 2018. Estimation of terrestrial radionuclide concentration and effect of soil parameters on exhalation and emanation rate of radon. J. Geochem. Explor. 184, 296–303.
- Jacob, P., H.G. Paretzke, H. Rosenbaum and M. Zankl, 1986. "Effective Dose Equivalents for Photon Exposures from Plane Sources on the Ground". Radiation Protection Dosimetry, 14(4), 299–310.
- Kocher, D. C., & Sjoreen, A. L., 1985. Dose-rate conversion factors for external exposure to photon emitters in soil. Health Physics, 48(2), 193–205.
- La Verde, D'Avino, V., Sabbarese, C., Ambrosino, F., Roca, V., Raulo, A., Pugliese, M., 2020. Radiation protection legislation and sustainable development of a rural green tuff village of Ischia Island. Sustainability 12 (20), 8374. Raslan, M.F., Haroun,
- Moustafa AR., 2002. Controls on the geometry of transfer zones in the Suez Rift and NW Red Sea: implications for the structural geometry of rift systems. AAPG Bull 86:979–1002.
- Omar AE., 2016. Geo-environmental and radioactivity assessment of East Abu Zenima area, Southwestern Sinai, Egypt, using remote sensing and GIS. Ph.D. Thesis, Suez Canal University Egypt, p260.
- Omar AE., 2021. Application of geospatial approaches to prospect radioactive minerals in the Um Bogma Younger Granites, Southwestern Sinai. Egypt Arab J Geosci. https://doi. Org/ 10. 1007/s12517- 021-06684-5.
- Omar AE, Arnous MO, El-Ghawaby MA, Ashami AS, El Zalaki MA. 2016a. Seismotectonic hazards assessment in Southwestern Sinai area using remote sensing and GIS. J Appl Sci 5:427–442. https://doi.org/10.21608/sinjas.2016.786.
- Omar AE, Arnous MO, El-Ghawaby MA, Ashami AS, El Zalaki MA. 2016b. Flash flood hazard mapping of wadi Baba basin Southwestern Sinai. Egypt J Appl Sci 5:409–426. https://doi.org/10.21608/sinjas. 2016.78663

- OMRAN, A., 2006.Geo-Environmental studies of North Western Gulf of Suez region, Egypt, M. Sc. Thesis, Suez Canal University, Faculty of Science, Geology Department, Ismailia.
- Ravisankar, R., Chandramohan, J., Chandrasekaran, A., Prakash, J.P., Vijayalakshmi, I., Vijayagopal, P., Venkatraman, B., 2015. Assessments of radioactivity concentration of natural radionuclides and radiological hazard indices in sediment samples from the East coast of Tamilnadu, India with statistical approach. Mar. Pollut. Bull. https://doi.org/10.1016/j.marpolbul.2015.05.058.
- Saad, A.M., Sakr, M.A.H., Omar, A.E., Temsah, Y.A., 2020. Assessment of radioactivity and geotechnical characteristics of soil foundation for suitability of safe urban extension using geospatial technology New SahlHasheesh Marin Port, Eastern Desert, Egypt. J. Environ. Analy. Chem. https://doi.org/10.1080/ 03067319.2020.1802444.
- Said R., 1962. The geology of Egypt. Elsevier Publishing Co., Amsterdam, p 396.
- Said, R., 1990. The Geology of Egypt. Balkema, Rotterdam, p. 1–721.
- Sakr, M.A.H., Omar, A.E., Saad, A.M., Moayedi, Hossein, 2021. Geotechnical parameters modelling and the radiation safety of expansive clayey soil treated with waste marble powder: a case study at west Gulf of Suez, Egypt. Environ. Earth Sci. 80, 263
- Salama, E., Diab, H. M., El-Khatib, A. M., & Ibrahim, A, 2015. Distribution of radionuclides in soil and beach samples of the western coast of Suez Gulf, Egypt. Arab Journal of Nuclear Science and Applications, 48(2), 63–69.
- Strougo, A., Abdallah, A.M., 1990. Mokattamian stratigraphy of north central EasternDesert (South of Maadi-Qattamiya road). Faculty of Science, Ain ShamsUniversity.
- Taylor, K.G., Owens, P., 2009. Sediments in urban river basins: a review of sediment-contaminant dynamics in an environmental system conditioned by human activities. J. Soils Sediments 9, 281–303.
- UNSCEAR, 2000. United Nations Scientific Committee on the Effects of Atomic Radiation, Report of UNSCEAR to the General Assembly, United Nations, New York, USA. pp. 111–125.
- UNSCEAR Sources and Effects Of, 2010.UNSCEAR Sources and Effects of Ionizing Radiation Exposures of the Public and Workers from Various Sources of Radiation UNSCEAR 2008 Report, 2010. New York.
- Uosif, M. A. M., & Abdel-Salam, L. M. 2011. An assessment of the external radiological impact in granites and pegmatite in central Eastern Desert in Egypt with elevated natural radioactivity. *Radiation Protection Dosimetry, 147(3), 467–473. https://doi.org/10.1093/rpd/ncq448.